Amplitude- versus frequency-modulated pumping light for coherent population trapping resonances at high buffer-gas pressure

A. B. Post, Y.-Y. Jau, N. N. Kuzma, and W. Happer

Department of Physics, Princeton University, Princeton, New Jersey 08544, USA

Coherent population trapping (CPT) signals can be optimized with amplitude-modulated pumping light. As shown theoretically and experimentally in this paper, the optimum wave forms produce strong CPT signals at both low buffer-gas pressures, where the hyperfine structure (HFS) splitting of the optical absorption lines is well resolved, and also at high buffer-gas pressures, where the HFS is no longer optically resolved due to pressure broadening. On the other hand, CPT resonances from frequency-modulated waves are severely degraded for these high-pressure conditions. High buffer-gas pressures may offer advantages for miniature frequency standards and magnetometers, including suppression of diffusion losses in miniature cells, suppression of light shifts, and less stringent requirements for frequency stability of the pumping light sources.

PACS number(s): 32.10.Fn, 33.20.Bx, 06.30.Ft

I. INTRODUCTION

Resonant light, modulated at the Bohr frequencies of transitions between certain ground-state sublevels of atoms, can induce coherences between the sublevels and cause the light absorption to change [1,2]. These *coherent population trapping* (CPT) resonances [3,4] have potential advantages for optically pumped frequency standards and magnetometers because they eliminate the need for an oscillating magnetic field [5].

For CPT applications in atomic clocks, the carrier frequency ω_c of the pumping light is chosen to be nearly equal to the optical resonance frequency ω_o for the $D1$ or $D2$ absorption lines of alkali-metal atoms. The light is usually modulated by an electro-optic crystal or by modulating the current of a diode laser. The modulation frequency Ω_m is often chosen to be half the Bohr frequency Ω for the transition (the "clock resonance") between the two ground-state sublevels with azimuthal quantum numbers $m_f = 0$. Denote the corresponding Bohr period by $T = 2\pi/\Omega$. The light has nearly pure frequency modulation (FM) and can be characterized by an FM modulation index m, such that the sidebands at the frequencies $\omega_c + q\Omega_m$ have amplitudes $J_q(m)$, where J_q is the Bessel function of order $q = 0, \pm 1, \pm 2, \ldots$.

The modulated light enters a cell containing alkali-metal atoms and a buffer gas of sufficiently low pressure such that the pressure-induced damping rate γ_o of the optical coherence is smaller than Ω. Assuming phase modulation at the frequency $\Omega_m = \Omega/2$, an FM modulation index $m = 1.84$ maximizes the power in the first-order sidebands at the frequencies $\omega_c \pm \Omega_m$. The sideband frequencies are approximately equal to the resonant absorption frequencies $\omega_o \pm \Omega/2$ of ground-state alkali-metal atoms in the upper and lower sublevels of the clock resonance. Under these conditions, coherent, resonant Raman scattering of photons between the first-order sidebands generates a coherent superposition between the initial and final energy sublevels of the clock resonance. The superposition state is called a *dark state* if the opacity of the atoms, averaged over a few optical cycles, is less than that of unpolarized atoms.

Many experiments [4,6] have confirmed that the amplitudes of CPT resonances generated by FM light decrease as γ_o grows with increasing buffer-gas pressure. At low pressures, where $\gamma_o < \Omega$, the instantaneous frequency of the light can sweep through resonance at times when atoms in the superposition state have minimum polarizability and, therefore, absorb little light. At higher pressures where $\gamma_o > \Omega$, an FM wave with maximized first-order sidebands will produce a barely visible CPT resonance, since the excursion of the instantaneous frequency remains within the pressure-broadened linewidth.

As a quantitative measure of the strength of CPT resonances we define the *saturation* $\mathcal{S}$ by

$$\mathcal{S} = 1 - \frac{P_d}{P_u}. \tag{1}$$

The quantity measured by the saturation can be understood with reference to Fig. 1. As shown in the top panel (a), an atomic vapor is pumped by light modulated at the pth subharmonic of the Bohr frequency Ω. For frequency-modulated light, it is convenient to choose $p = 2$. The response time of the detector is not fast enough to detect power fluctuations at optical or microwave frequencies, but we assume that the detector is fast enough to detect much slower transient changes in the opacity of the vapor, due to the relaxation times of CPT resonances. In the middle panel [Fig. 1(b)], the top trace $P = P_0$ denotes the transmitted power for the light that is well detuned from optical resonance, $|\omega_c - \omega_o| \gg \gamma_o$, and for which the absorption by the vapor is negligible. The lower trace shows the transmitted power for the optically resonant light with $\omega_c = \omega_o$. From time t_0 to t_1, the modulation frequency is well detuned from the CPT resonance — that is, $|p\Omega_m - \Omega| \gg \Gamma$, where Γ is the relaxation rate of the CPT resonance. No coherence is induced within the ground-state sublevels of the vapor, although optical pumping by the light may introduce some steady-state population imbalances. We denote the power absorbed by these noncoherent atoms by P_u.
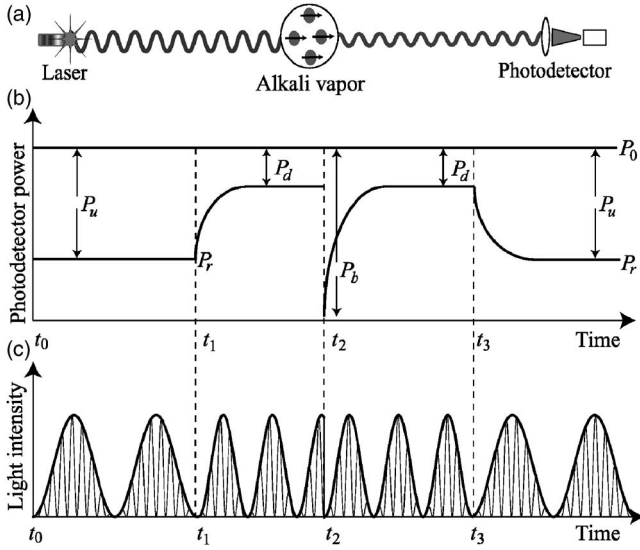
FIG. 1. (a) A CPT gedanken experiment. (b) Transmitted optical powers: P_0 for light detuned from the optical absorption line, $|\omega_c - \omega_o| \gg \gamma_o$, and P_r for optically resonant light with $\omega_c - \omega_o = 0$. (c) Light modulation format, taken to be amplitude modulated for clarity, on the same time scale as (b). The long modulation period is a microwave period, and the short period (not to scale) represents an optical period.

At time t_1, the modulation frequency is switched to CPT resonance, so that $p\Omega_m = \Omega$. After a transient time on the order of $1/\Gamma$ (not to scale in the figure), the atoms are pumped into a superposition state oscillating in phase with the modulated light. The power P_d absorbed by the atoms is minimized. This is the *dark state*, and we say that the pumping light is modulated as a *dark wave* for this superposition state.

Imagine that a time delay of half a Bohr period $T/2$ is suddenly introduced into the modulation pattern of the pumping light at the time t_2, leading to an instantaneous modulation phase shift shown in Fig. 1(c). Immediately following this phase shift, the relative phase between the oscillating superposition state and the modulated light is such that the absorbed power P_b is at a maximum. This *bright-state* absorption is only transient. After a time on the order of $1/\Gamma$ the atoms are optically pumped into a new dark state that differs by 180° in phase from the original dark state. The absorbed power again becomes P_d.

The saturation $\mathcal{S}$ of Eq. (1) is a useful parameter for specifying the strength of the CPT resonance since it is nearly independent of the cell optical depth for optically thin cells. The saturation $\mathcal{S}$ can be measured or calculated for light with an arbitrary distribution of sidebands.

In Sec. II we begin our discussion of CPT with a fully classical model, a dipole antenna that rotates in space at the frequency $\Omega/2$. In Sec. III we show that the CPT response of the easy-to-visualize antenna of Sec. II is nearly equivalent to the CPT response of alkali-metal atoms to circularly polarized $D1$ pumping light. The correspondence is exact for buffer-gas pressures just large enough that the hyperfine splitting of the excited $^2P_{1/2}$ state is no longer optically resolved. Insights gained from the response of the classical

antenna of Sec. II are therefore quantitatively transferrable to the CPT signals for alkali-metal atoms.

The connection between the classical antenna and the atoms can be understood by considering the optical absorption cross sections of both systems. For a nonrotating dipole antenna, with the axis pointing along the unit vector $\mathbf{u}$, the classical absorption cross section for light with a linear polarization vector $\mathbf{e} = \mathbf{E}/E$ and an optical frequency ω is

$$\sigma = 2\sigma_0 (\mathbf{e} \cdot \mathbf{u})^2, \tag{2}$$

where the mean cross section for random orientations of $\mathbf{u}$ and $\mathbf{e}$ in the plane normal to the direction of propagation of the light is

$$\sigma_0 = \frac{2\pi r_e c f \gamma_o}{(\omega_o - \omega)^2 + \gamma_o^2}. \tag{3}$$

Here, $r_e = e^2/m_e c^2$ is the classical electron radius, c is the speed of light, γ_o is the optical coherence damping rate, and ω_o is the resonant absorption frequency. The oscillator strength, which is the mean value of $(\mathbf{e} \cdot \mathbf{u})^2$, is $f = 1/2$.

The quantum-mechanical cross section for optical absorption of $D1$ light by nonrotating alkali-metal atoms (that is, atoms with no hyperfine structure and no externally applied magnetic fields) is [7]

$$\sigma = \sigma_0 (1 - 2\mathbf{s} \cdot \langle \mathbf{S} \rangle), \tag{4}$$

where the photon spin is

$$\mathbf{s} = i\mathbf{e} \times \mathbf{e}^*. \tag{5}$$

The expectation value of the electron spin is $\langle \mathbf{S} \rangle$, and σ_0 is given by Eq. (3) with $f \approx 1/3$.

Although the cross-section expressions in Eqs. (2) and (4) look different, they are completely equivalent. Consider a Cartesian coordinate system with orthonormal unit vectors $\mathbf{x}$, $\mathbf{y}$, and $\mathbf{z}$. Let the light propagate along $\mathbf{z}$, and let both $\mathbf{u}$ and $\mathbf{e}$ be linear combinations of $\mathbf{x}$ and $\mathbf{y}$. The Poincaré pseudospin operators [8] for the xy plane can be chosen as

$$\overleftrightarrow{P}_\zeta = \frac{1}{2}(\mathbf{xx} - \mathbf{yy}),$$

$$\overleftrightarrow{P}_\xi = \frac{1}{2}(\mathbf{xy} + \mathbf{yx}),$$

$$\overleftrightarrow{P}_\eta = \frac{1}{2i}(\mathbf{xy} - \mathbf{yx}). \tag{6}$$

Dot products of Poincaré dyadics behave like spin-1/2 operators: for example, $\overleftrightarrow{P}_\xi \cdot \overleftrightarrow{P}_\eta - \overleftrightarrow{P}_\eta \cdot \overleftrightarrow{P}_\xi = i\overleftrightarrow{P}_\zeta$ and $\Sigma_\kappa \overleftrightarrow{P}_\kappa \cdot \overleftrightarrow{P}_\kappa = S(S+1)(\mathbf{xx} + \mathbf{yy})$, with $S = 1/2$. In Poincaré space, the cross section of Eq. (2) becomes

$$\sigma = \sigma_0 (1 - 2\mathbf{s}_P \cdot \langle \mathbf{S} \rangle_P), \tag{7}$$

an expression formally identical to Eq. (4). The electron pseudospin,

$$\langle \mathbf{S} \rangle_P = \mathbf{u} \cdot \overset{\leftrightarrow}{\mathbf{P}} \cdot \mathbf{u}, \tag{8}$$

is determined by the orientation direction $\mathbf{u}$ of the antenna. The photon pseudospin

$$\mathbf{s}_P = -2\mathbf{e} \cdot \overset{\leftrightarrow}{\mathbf{P}} \cdot \mathbf{e} \tag{9}$$

is determined by the linear polarization vector $\mathbf{e}$ of the light. One should remember, however, that the orthogonal axes ξ, η, and ζ of Poincaré space are not the same as the orthogonal axes x, y, and z of ordinary space.

Cross sections like those of Eqs. (2) and (4) have nulls for certain orientations of the antenna (or the atomic spin) with respect to the light and, therefore, correspond to systems with the maximum possible CPT signals. For example, the antenna cross section of Eq. (2) vanishes when $\mathbf{e} \cdot \mathbf{u} = 0$. This is because the polarization $\mathbf{e}$ of the electric field must have some projection along the antenna axis $\mathbf{u}$ for the field to drive current. It is common knowledge that the absorption cross section σ of a short dipole antenna vanishes if the direction $\mathbf{u}$ of the antenna axis is perpendicular to the direction $\mathbf{e}$ of the received field. For example, one can orient a transistor radio with a ferrite, magnetic dipole antenna to cancel out the reception of most of amplitude-modulated (AM) stations, which usually have magnetic fields that are approximately linearly polarized in a direction parallel to the ground.

The cross section [Eq. (4)] of the atom has a null when $2\mathbf{s} \cdot \langle \mathbf{S} \rangle = 1$ — that is, when the spin of the photon has its maximum magnitude $|\mathbf{s}| = 1$ and is parallel to the expectation value $\langle \mathbf{S} \rangle$ of the electron spin, which also has its maximum magnitude $|\langle \mathbf{S} \rangle| = 1/2$, so that $\langle \mathbf{S} \rangle = \mathbf{s}/2$. If the $D1$ photon were absorbed, the electronic angular momentum of the excited atom would be $\langle \mathbf{J} \rangle = \mathbf{s} + \langle \mathbf{S} \rangle = 3\mathbf{s}/2$ with magnitude $|\langle \mathbf{J} \rangle| = 3/2$. But the maximum electronic angular momentum for the $^2P_{1/2}$ upper state of the $D1$ transition is $|\langle \mathbf{J} \rangle| = 1/2$, so there is no way to accommodate the angular momentum of the absorbed photon. The null in the cross section of Eq. (4) thus comes from the conservation of angular momentum.

A nonrotating antenna or atom that is oriented to have a null in its directive gain for an unmodulated wave is in a *static dark state* for that wave. The unmodulated wave can be called a *static dark wave* for the static dark state. An example of static dark states and dark waves is an antenna and a wave for which $\mathbf{e} \cdot \mathbf{u} = 0$, with both $\mathbf{e}$ and $\mathbf{u}$ time independent. If the antenna rotates or if the atom has nuclear hyperfine interactions or is exposed to an externally applied magnetic field, the direction of the null in the directive gain also rotates. CPT is a way to exploit these periodic nulls with modulated waves, or *periodic dark waves*, that have peak amplitudes or exactly resonant frequencies when the directive gain has a null. There is very little absorption of the dark waves by the rotating antenna or atom. The corresponding state of the antenna or atom is a *periodic dark state*.

As indicated in Fig. 1, if we delay the periodic dark wave by half a modulation period, the antenna or atom in the original periodic dark state will extract maximum power and will be in a *periodic bright state* with respect to the delayed wave. The wave will have its maximum amplitude or the

exact resonance frequency when the antenna axis is parallel to the electric field or when the spins of the photon and atom are antiparallel. In Sec. III, we use these facts to explain why AM light of fixed modulation index continues to give good CPT signals at high gas pressures, whereas the CPT signals from FM light of fixed modulation index become impractically small as the gas pressure increases.

The cross section for optical absorption of $D2$ light by alkali-metal atoms with no hyperfine structure is [7]

$$\sigma = \sigma_0 (1 + \mathbf{s} \cdot \langle \mathbf{S} \rangle), \tag{10}$$

where σ_0 is given by Eq. (3), with $f \approx 2/3$. There is no relative orientation of the photon spin $\mathbf{s}$ and the electron spin $\langle \mathbf{S} \rangle$ that reduces the cross section in Eq. (10) to zero. There are no true dark states for $D2$ pumping, and the best one can do is to obtain a factor of 3 in the ratio of maximum to minimum absorption rates.

In Sec. IV we show that there are unique dark waves that minimize the required laser power and maximize the saturation of 0-0 CPT resonances excited with circularly polarized $D1$ light. For low gas pressures, where $\gamma_o < \Omega$, this *optimum wave* consists of two monochromatic waves, with frequencies differing by Ω. One frequency resonantly excites atoms in the upper sublevel of the 0-0 state, and the other frequency resonantly excites atoms in the lower sublevel. For buffer-gas pressures that are high enough so that $\gamma_o \geq \Omega$, the optimum is a series of pulses, modulated with nearly Gaussian envelopes. The required number of sidebands of the pulse train is proportional to the square root of the gas pressure.

In Sec. V we show that the optimum CPT waves can be converted into optimum waves for push-pull pumping [9], by splitting the light into two beams, delaying one beam by half a hyperfine period $T/2$, polarizing the two beams to opposite circular polarizations, and recombining them. This makes the circular polarization of the exciting light alternate at the frequency Ω and ensures that atoms are not pumped to the end states, which is a serious problem [10] for the conventional approaches using a fixed (nonalternating) circular polarization. For low gas pressures, where $\gamma_o < \Omega$, the two frequency components of the combined wave are linearly polarized at right angles to each other. This low-pressure, optimum wave has been called "lin-$\perp$-lin" by Zanon *et al.* [11], and it is the same as the modulation format used by Jau *et al.* in their first report of push-pull pumping [9]. For higher pressures, where the optimum CPT wave has many sidebands, the corresponding sidebands of the push-pull wave have alternating linear polarizations.

In Sec. VI we present the data that validate the previous discussions. We report measurements of CPT signals from five Rb cells of varying buffer-gas pressure, using both AM and FM light. As expected, the CPT saturation decreases with higher buffer-gas pressure. The degradation of the saturation due to pressure broadening is far more pronounced with FM light than it is with AM. With AM light, good CPT signals can be detected in cells with two atmospheres of buffer gas pressure, where the optical broadening far exceeds the hyperfine splitting.
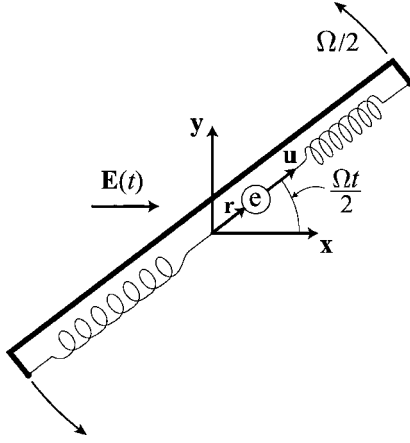
FIG. 2. Dipole antenna, modeled as an electron driven to oscillate along an axis **u** by an electric field **E**(*t*). The electron is attached to two springs, the ends of which are fixed on a rigid frame rotating in the *xy* plane with angular velocity $\Omega/2$, such that the angle between the frame axis **u** and the **x** axis is given by $\Omega t/2$.

II. CLASSICAL DIPOLE ANTENNA

As the simplest antenna, we consider an elastically bound electron with charge $-e$ and mass m_e. The electron is constrained to move along the direction of the unit vector

$$\mathbf{u} = \mathbf{x} \cos(\Omega t/2) + \mathbf{y} \sin(\Omega t/2). \quad (11)$$

Here **x** and **y** are the fixed orthonormal basis vectors. The electron is connected to two springs with fixed end points and a resonant frequency of ω_o, as sketched in Fig. 2. At time $t=0$, $\mathbf{u}=\mathbf{x}$, and **u** is rotating with angular velocity $\Omega/2$ in the *xy* plane. Taking the unit vectors of Poincaré space to be $\boldsymbol{\xi}$, $\boldsymbol{\eta}$, and $\boldsymbol{\zeta}$ we find that the electron pseudospin, Eq. (8), of the antenna rotates about the axis η at twice the frequency of the antenna in real space,

$$\langle \mathbf{S} \rangle_P = \frac{1}{2}(\boldsymbol{\zeta} \cos \Omega t + \boldsymbol{\xi} \sin \Omega t). \quad (12)$$

From Newton's second law, the motion of the electron is determined by the differential equation

$$m_e \frac{d^2 r}{dt^2} = -kr - 2\gamma_o m_e \frac{dr}{dt} - eE_u, \quad (13)$$

where $\mathbf{r}=r\mathbf{u}$ is the displacement of the electron from the central equilibrium point, the restoring force constant is k, and the damping coefficient is γ_o. For a real dipole antenna, γ_o would be determined by a combination of the radiation resistance and the coupling of the antenna to the receiving circuit. For atoms, which we discuss in the next section, the damping rate γ_o is normally due to pressure broadening of the optical absorption line of the atoms by the buffer gas.

We write $E_u = \mathbf{E} \cdot \mathbf{u}$ (the projection of the externally applied electric field along **u**) and r as Fourier integrals:

$$E_u = \int_{-\infty}^{\infty} d\omega \widetilde{E}_u(\omega) e^{-i\omega t}, \quad r = \int_{-\infty}^{\infty} d\omega \widetilde{r}(\omega) e^{-i\omega t}. \quad (14)$$

Substituting Eq. (14) into Eq. (13) gives the Fourier amplitude of r,

$$\widetilde{r}(\omega) = \frac{-e\widetilde{E}_u(\omega)}{k - 2i\gamma_o m_e \omega - m_e \omega^2}. \quad (15)$$

The dipole moment of the antenna is

$$\boldsymbol{\mu} = -e\mathbf{r} = -er\mathbf{u} = \mu_u \mathbf{u}. \quad (16)$$

The Fourier amplitude of μ_u is

$$\widetilde{\mu}_u = -e\widetilde{r} = \alpha \widetilde{E}_u. \quad (17)$$

From Eqs. (15) and (17) we see that the polarizability α is

$$\alpha(\omega) = \frac{-e^2}{m_e(\omega - \omega_o + i\gamma_o)(\omega + \omega_o + i\gamma_o)}$$

$$\approx \left(\frac{r_e c^2 f}{\omega_o}\right) \frac{1}{\omega_o - \omega - i\gamma_o}. \quad (18)$$

The "one-pole" approximation to α on the second line of Eq. (18) is excellent for conditions of interest to us, where $\gamma_o \ll \omega_o$ and ω is close to the resonant frequency:

$$\omega_o = \sqrt{\frac{k}{m_e} - \gamma_o^2}. \quad (19)$$

The mean oscillator strength for the dipole antenna is $f = 1/2$.

Consider a monochromatic electric field of carrier frequency ω_c polarized along the *x* axis. Then $\mathbf{E} = E_x \mathbf{x}$, where

$$E_x = E^{(0)} e^{-i\omega_c t}. \quad (20)$$

Since the polarization of the field is $\mathbf{e}=\mathbf{x}$, the photon pseudospin, Eq. (9), is

$$\langle \mathbf{s} \rangle_P = -\boldsymbol{\zeta}. \quad (21)$$

The projection $E_u = \mathbf{u} \cdot \mathbf{x} E_x$ will have frequencies $\omega_c \pm \Omega/2$ and will induce corresponding frequency components of the dipole moment, in accordance with Eq. (17). The projection of the rotating dipole on the *x* axis will therefore have three frequency components: the original carrier frequency ω_c and two sidebands with frequencies $\omega_c \pm \Omega$. So the projection of the dipole moment induced by the monochromatic wave of Eq. (20) along the *x* axis can be written as

$$\mu_x = \alpha_{xx}(\omega_c, t) E^{(0)} e^{-i\omega_c t}, \quad (22)$$

where the *xx* component of the time-dependent polarizability tensor is

$$\alpha_{xx}(\omega, t) = \frac{\alpha(\omega + \Omega/2)}{4}(1 + e^{-i\Omega t}) + \frac{\alpha(\omega - \Omega/2)}{4}(1 + e^{i\Omega t}). \quad (23)$$

From inspection of Eq. (23) we find that the polarizability vanishes at times when $\Omega t = \pm\pi, \pm 3\pi, \pm 5\pi, \dots$. These are the times when $\mathbf{u} = \pm\mathbf{y}$ and the directive gain of the antenna vanishes.

By modulating the monochromatic wave of Eq. (20) such that it has peak amplitudes (AM) or exactly resonant frequencies (FM) at the null times, we can make dark waves for the rotating antenna. We write the modulated wave as

$$E_x = \sum_q E^{(q)} e^{-i\omega_q t}. \tag{24}$$

The sideband index is $q = 0, \pm 1, \pm 2, \ldots$, $\widetilde{E}^{(q)}$ is the Fourier amplitude, and the sideband frequency is

$$\omega_q = \omega_c + q\Omega/2. \tag{25}$$

Combining Eq. (24) with Eq. (17) we find the induced dipole moment

$$\mu_x = \sum_q \alpha_{xx}(\omega_q, t) E^{(q)} e^{-i\omega_q t}. \tag{26}$$

The mean power absorbed by the dipole is

$$P = \left\langle E_x^* \frac{d\mu_x}{dt} \right\rangle + \text{c.c.} \tag{27}$$

The angular brackets denote a time average over one modulation period, and "c.c." denotes a complex conjugate. Substituting Eqs. (24) and (26) into Eq. (27) we find

$$P = \frac{\omega_o}{2} \sum_q \alpha''(\omega_q) |E^{(q+1)} + E^{(q-1)}|^2, \tag{28}$$

where $\alpha''(\omega_q)$ denotes the imaginary part of Eq. (18).

As a specific example, consider a resonant, phase-modulated wave for which Eq. (24) can be written as

$$E_x = K e^{-i[\omega_c t + m \cos(\Omega\{t-t_0\}/2)]}, \tag{29}$$

where K is a constant amplitude. The instantaneous frequency,

$$\omega = \omega_c - \frac{m\Omega}{2} \sin(\Omega\{t-t_0\}/2), \tag{30}$$

which is the rate of change of the phase of Eq. (29), is equal to the resonant frequency ω_o when $t = t_0$. We can think of t_0 as an adjustable delay time that can be used to transform a dark wave to a bright wave or vice versa.

From the generating function of Bessel functions [12] we find that the sideband amplitudes of Eq. (29) are

$$E^{(q)} = K J_q(m) e^{iq(\Omega t_0 - \pi)/2}, \tag{31}$$

where $J_q(m)$ is a Bessel function of order q and argument m, and $E^{(q)}$ was defined in Eq. (24).

For a typical phase modulator, such as an electro-optic modulator based on LiNbO$_3$, the modulation index m will be a real parameter that is proportional to the peak modulating voltage and the length of the crystal. In this case, the phase modulator produces pure frequency modulation and the instantaneous frequency ω of Eq. (30) is real. It oscillates between the bounds $\omega_c \pm m\Omega/2$ at the modulation frequency $\Omega/2$. We will generalize the concept of phase modulation by assuming that m can be an arbitrary complex number, m

$= m' + im''$. A purely real modulation index $m = m'$ describes FM, and a purely imaginary modulation index $m = im''$ is a good approximation for AM.

For light with its carrier tuned to the optical resonance frequency ($\omega_c = \omega_o$) and for generalized phase modulation, with sideband amplitudes given by Eq. (31), the absorbed power Eq. (28) becomes

$$P = \mathcal{A} \sum_q \frac{|J_{q+1} e^{i\Omega t_0/2} - J_{q-1} e^{-i\Omega t_0/2}|^2}{(q\Omega/2)^2 + \gamma_o^2} = P_u + P_1 \cos(\Omega t_0 + \psi). \tag{32}$$

The coefficient $\mathcal{A}$ is

$$\mathcal{A} = \frac{r_e c^2 f \gamma_o |K|^2}{2}. \tag{33}$$

The phase ψ of Eq. (32) depends on the modulation index m and the ratio γ_o/Ω of the optical damping rate to the resonance frequency Ω. Expressions for the mean power $P_u \geq 0$ absorbed by an unpolarized ensemble of antennas, oriented at random in the xy plane, and the phase-dependent power $P_1 \geq 0$ can readily be found from the first line of Eq. (32). The bright and dark powers, discussed in Fig. 1, are $P_b = P_u + P_1$ and $P_d = P_u - P_1$. The saturation defined in Eq. (1) is

$$\mathcal{S} = 1 - \frac{P_d}{P_u} = \frac{P_1}{P_u}. \tag{34}$$

For the low-pressure limit (when $\gamma_o \ll \Omega$), the terms in the sum of Eq. (32) with $q \neq 0$ can be neglected and the sum is well approximated by

$$P = 4\mathcal{A} |J_1(m) \cos(\Omega t_0/2)|^2 / \gamma_o^2. \tag{35}$$

In this case $P_u = P_1 = 2\mathcal{A} |J_1(m)|^2 / \gamma_o^2$ and $\psi = 0$. If one varies the time delay t_0 of the pumping wave from Eq. (29), the absorbed power will oscillate between a maximum value $P_b = P_u + P_1 = 4\mathcal{A} |J_1(m)|^2 / \gamma_o^2$ for the bright wave and a minimum value $P_d = P_u - P_1 = 0$ for the dark wave. Almost any nonzero modulation index m will work at low gas pressure: FM with $m = m^* \neq j_{1,s}$, where $j_{1,s}$ is one of the zeros [12] of J_1; AM with $m = -m^*$; or some combination when m has both real and imaginary parts. The saturation approaches the limit $\mathcal{S} = 1$.

We can also sum Eq. (32) for high gas pressures where $\gamma_o \gg |m|\Omega$. Since $J_q(m)$ rapidly approaches zero for $q > |m|$, we can make the replacement $\gamma_o^2 + (q\Omega/2)^2 \rightarrow \gamma_o^2$ for those values of q where the Bessel functions in the numerator are not negligibly small. Then Eq. (32) becomes

$$P = \frac{\mathcal{A}}{\gamma_o^2} \sum_q \left[|J_{q+1}|^2 + |J_{q-1}|^2 - J_{q+1} J_{q-1}^* e^{i\Omega t_0} - J_{q+1}^* J_{q-1} e^{-i\Omega t_0} \right]$$

$$= \frac{2\mathcal{A}}{\gamma_o^2} [J_0(i2m'') - J_2(i2m'') \cos(\Omega t_0)], \tag{36}$$

where the imaginary part of the modulation index is

$$m'' = \frac{1}{2}(m - m^*). \tag{37}$$

In evaluating Eq. (36) we made use of the identity

$$\sum_q J_{n+q}(m)J_q(m^*) = J_n(m - m^*), \tag{38}$$

which can be verified by considering the Bessel expansion of $e^{im \sin \theta}(e^{im \sin \theta})^*$. We also noted that J_2 has negative real values and J_0 has positive real values for arguments along the imaginary axis. Using Eq. (36) in Eq. (34) we find that the saturation for a fixed modulation index in the high-pressure limit is

$$\mathcal{S} = -\frac{J_2(i2m'')}{J_0(i2m'')}. \tag{39}$$

For FM light m is real, $m''=0$, $J_0(0)=1$, and $J_2(0)=0$, so Eq. (39) becomes $\mathcal{S}=0$.

In deriving Eq. (39) we assumed a fixed modulation index m. If the modulation index $m=m^*$ for FM light increases with pressure, one can limit the loss of saturation. For AM light with a fixed imaginary value of m, the saturation never falls below that given by Eq. (39). For example, if we take $m''=1$ in Eq. (39), we find that the saturation never falls below $\mathcal{S}=0.302$, no matter how much line broadening there is.

More insight into the pressure dependence of CPT signals for FM and AM waves can be gained from a detailed consideration of a few representative cases. The electric fields [Eq. (31)] of dark (solid line) and bright (dash-dotted line) FM waves with $m=1$ are illustrated in Fig. 3(a). The phases $\Omega t_0/2$ of the bright and dark waves differ by $\pi/2$. The antenna is assumed to have relatively little damping, with $\gamma_o/\Omega=0.2$. Figure 3(b) shows the resulting antenna currents, the time derivatives of the dipole moments given by Eq. (26). Figure 3(c) plots the absorbed powers of Eq. (27), which are the products of the curves in panels (a) and (b). Figure 3(d) illustrates the relative deviation $(\omega-\omega_c)/\gamma_o$ of the instantaneous frequency of Eq. (30) from the carrier frequency $\omega_c=\omega_o$. It is superimposed on a series of arrows indicating the orientation of the antenna at successive times. When **u** is pointing along the horizontal direction (parallel or antiparallel to **x**), the antenna absorbs maximum power from the bright wave, for which the instantaneous frequency ω of Eq. (30) is exactly equal to the resonant frequency ω_o of the nonrotating antenna. Much less power is absorbed from the dark wave, for which the instantaneous frequency ω has maximum detuning. The detuning greatly limits the amount of power that can be absorbed from the dark wave because the resonance line is much narrower than the maximum frequency excursion, $m\Omega/2=\Omega/2$. Half a modulation cycle later, when the instantaneous frequency of the dark wave is on resonance, the antenna is perpendicular to the electric field direction, and the field is unable to drive current, even though it has the exact resonant frequency. The bright wave is also not absorbed, both because of the orthogonality of the antenna to the field and because the frequency of the bright wave has maximum detuning at such times. Immediately af-
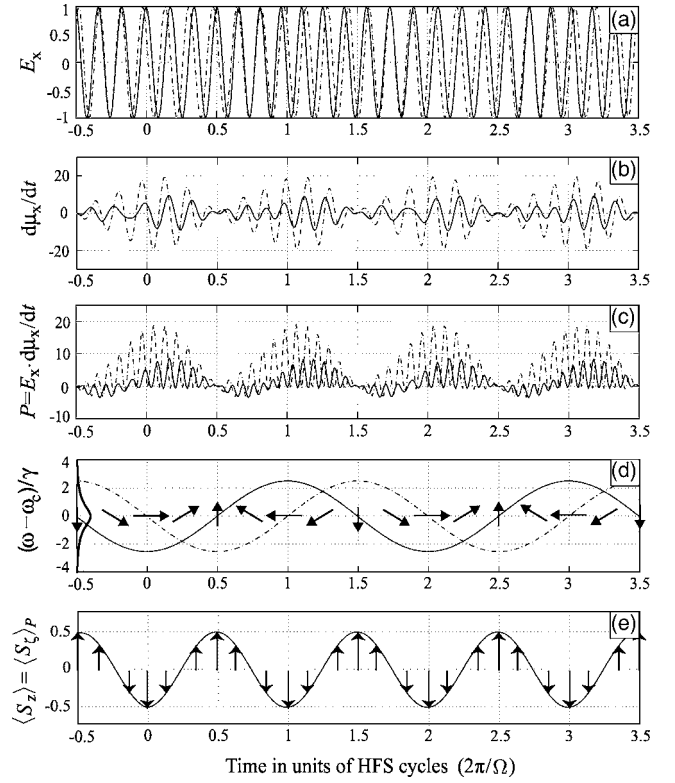

FIG. 3. CPT at low buffer-gas pressure with FM light. The electric fields E_x of the dark (solid) and bright (dash-dotted) waves are shown in (a). Panel (b) shows the corresponding antenna currents $d\mu_x/dt$; the dissipated power $E_x \cdot d\mu_x/dt$ is shown in (c). Panel (d) has sketches of the antenna orientations at various times. Horizontal orientations are parallel to the driving field $E_x\mathbf{x}$, and vertical orientations are perpendicular. Also shown in (d) are the instantaneous, relative frequency detunings $(\omega-\omega_c)/\gamma$ of the bright and dark waves, compared to the absorption profile of the antenna (thick solid line plotted vertically). Panel (e) shows the average electronic spin $\langle S_z \rangle$ of an alkali-metal atom rotating at Ω. The electronic spin (solid line) is equal to the Poincaré spin $\langle S_\zeta \rangle_P$ of the antenna (vertical arrows). The $D1$ cross section of the alkali atoms has nulls at $\langle S_z \rangle = 1/2$, which occur at the same times as the antenna nulls. The relative absorption-line broadening is $\gamma_o/\Omega=0.2$, the phase modulation index is $m=1$, and the resulting CPT saturation is $\mathcal{S}=0.595$.

ter the antenna is oriented perpendicularly to the field, the power pulses are negative. This represents transfer of power stored in the antenna oscillations back into the field. The average power over any modulation period, $2\pi/\Omega$, remains positive. The saturation is $\mathcal{S}=0.595$, somewhat less than the narrow-line limit $\mathcal{S}=1$, because the damping rate γ_o is 20% of Ω and is not completely negligible.

All parameters of Fig. 4 are the same as those of Fig. 3, except that the modulation index is $m=i$ rather than $m=1$ as for Fig. 3. As can be seen in Fig. 4(a), there are now bright and dark AM waves, delayed by half a hyperfine cycle with respect to each other. The real part of the instantaneous frequency in Eq. (30) is constant and equal to the resonant frequency ω_o of the nonrotating dipole at all times. However, the amplitude of the bright wave is maximum when the field and antenna are parallel, so the antenna can respond most efficiently. For the dark wave, the field is maximum when the
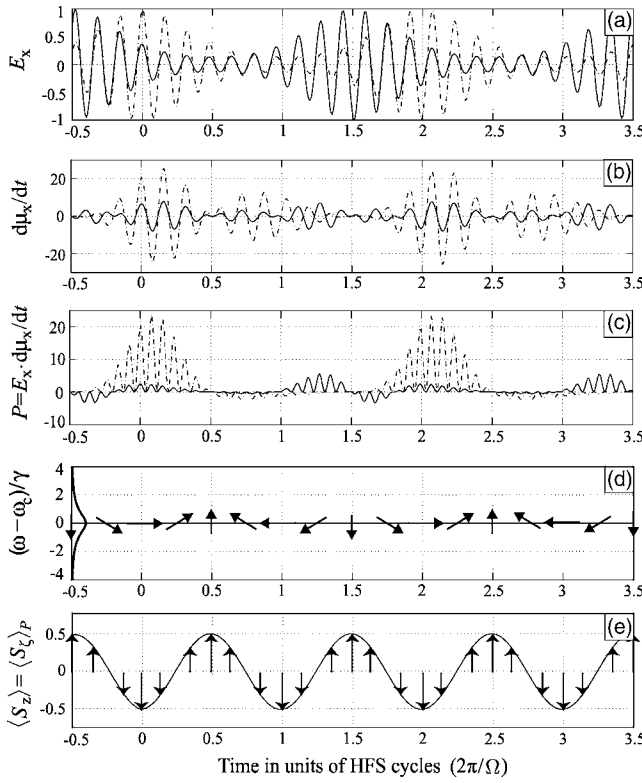
FIG. 4. CPT at low pressure with AM light. The quantities plotted in each panel are the same as those of Fig. 3. The relative absorption-line broadening is $\gamma_o/\Omega=0.2$, the phase modulation index is $m=i$, and the resulting CPT saturation is $\mathcal{S}=0.662$.
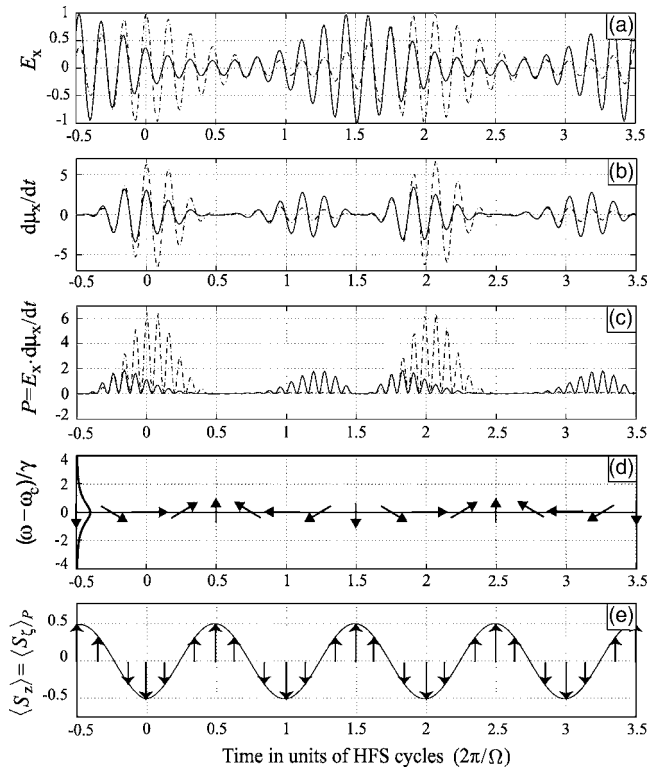

FIG. 5. CPT at high pressure with AM light. The quantities plotted in each panel are the same as those of Fig. 3. The relative absorption-line broadening is $\gamma_o/\Omega=2$, the phase modulation index is $m=i$, and the CPT saturation is $\mathcal{S}=0.316$.

field and antenna are perpendicular, so it is not possible to drive any current at that point. There is therefore less excitation of the antenna with the dark wave than with the bright wave. The saturation is $\mathcal{S}=0.662$, a bit larger than that for the FM wave of Fig. 3, but less than the narrow-line limit $\mathcal{S}=1$, because the damping rate is not completely negligible.

All parameters of Fig. 5 are the same as those of Fig. 4 except that there is relatively fast damping with $\gamma_o/\Omega=2$. The saturation has dropped from $\mathcal{S}=0.662$ in Fig. 4 to $\mathcal{S}=0.316$, nearly to the infinite broadening limit, 0.302 of Eq. (39) for $m=i$. The signal saturation for AM waves does not have a strong dependence on γ_o. The ratio of bright-wave power to dark-wave power is smaller for Fig. 5 than for Fig. 4 because the broader absorption cross section allows for more absorption of dark-wave light when the antenna is not quite perpendicular to the field. We note that as $m''\to\infty$, $-J_2(i2m'')/J_0(i2m'')\to 1$, so for high gas pressure we can recover 100% saturation by using AM light that is modulated as a series of pulses that are very short compared to the rotation period of the spring. If the pulses of the dark wave arrive just as the dipole and antenna are perpendicular, almost no power will be absorbed. However, the pulse of the bright wave arrives at the antenna when it is parallel to the electric field, so much more power will be absorbed.

All parameters of Fig. 6 are the same as in Fig. 5 except that $m=1$, rather than $m=i$. There are FM bright and dark waves, just like those of Fig. 3. However, since the relative line broadening is large ($\gamma_o/\Omega=2$), the relative frequency

detuning from resonance is too small for the dark wave (when the field is parallel to the antenna) to make much difference in the absorption. This can be seen in panel (d) of Fig. 6. Both the bright and dark waves have instantaneous frequencies close to the center of the broad resonance response curve at all times, and they have nearly the same absorptions. The saturation drops to $\mathcal{S}=0.016$, a very serious loss.

III. QUANTUM-MECHANICAL POLARIZABILITY

Here we show that the response of an alkali-metal atom to circularly polarized $D1$ light is formally identical to the response of a classical dipole antenna to linearly polarized light, the details of which we discussed in the previous section. In analogy to Eq. (26), the expectation value of the dipole moment $\langle\tilde{\boldsymbol{\mu}}(\omega,t)\rangle$ induced in the alkali-metal atom at time t by the Fourier component $\tilde{\mathbf{E}}(\omega)$ of the electric field of the light is

$$\langle\tilde{\boldsymbol{\mu}}(t)\rangle = \int_{-\infty}^{\infty} d\omega \langle\tilde{\overline{\alpha}}(\omega,t)\rangle\cdot\tilde{\mathbf{E}}(\omega). \qquad (40)$$

The polarizability dyadic is the expectation value of the polarizability operator with respect to the ground-state density matrix $\rho=\rho(t)$ of the atoms,
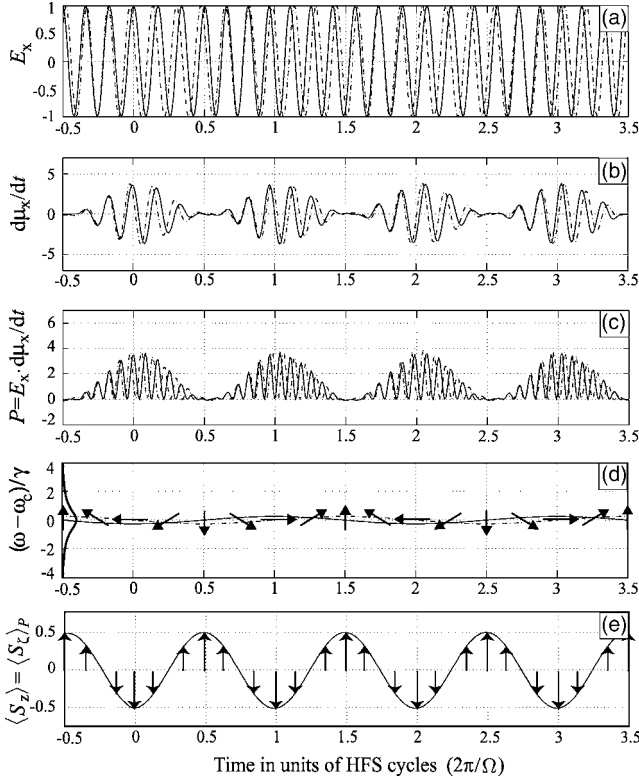
FIG. 6. CPT at high buffer-gas pressure with FM light. The quantities plotted in each panel are the same as those of Fig. 3. The relative absorption-line broadening is $\gamma_o/\Omega = 2$, the phase modulation index is $m=1$, and the CPT saturation is $\mathcal{S} = 0.0016$.

$$\langle\vec{\alpha}(\omega,t)\rangle = \text{Tr}[\vec{\alpha}(\omega)\rho(t)]. \tag{41}$$

The matrix elements between ground-state sublevels $|\mu\rangle$ and $|\nu\rangle$ of the polarizability operator are time independent and given by [7]

$$\vec{\alpha}_{\mu\nu}(\omega) = \frac{1}{\hbar}\sum_k \frac{\boldsymbol{\mu}_{\mu k}\boldsymbol{\mu}_{k\nu}}{\omega_{k\nu} - \omega - i\gamma_o}. \tag{42}$$

The energies of the ground-state sublevels are E_μ and E_ν, while k denotes the excited-state sublevels $|k\rangle$ with energies E_k. The Bohr frequencies are

$$\omega_{k\nu} = \frac{E_k - E_\nu}{\hbar}. \tag{43}$$

The optical coherence between the ground and excited states damps exponentially at the rate γ_o as a result of spontaneous radiative decay and collisions with other atoms. For very low buffer-gas pressures one has to account for Doppler broadening of the absorption line due to the velocity distribution of the atoms. But for most miniature atomic clocks the buffer-gas pressure is high enough (more than a few tens of Torr) so that the pressure broadening exceeds the Doppler broadening. We will therefore ignore Doppler broadening, although it is quite straightforward to include it [7].

It will be convenient to define a dimensionless excitation operator $\mathbf{A}^\dagger$ and a deexcitation operator $\mathbf{A}$, given by

$$\mathbf{A}_{k\nu}^\dagger = \frac{\boldsymbol{\mu}_{k\nu}}{\mu^*}, \quad \mathbf{A}_{\mu k} = \frac{\boldsymbol{\mu}_{\mu k}}{\mu}. \tag{44}$$

The amplitude of μ is defined by

$$|\mu|^2 = \frac{2\hbar r_e c^2 f}{\omega_o}, \tag{45}$$

where f is the oscillator strength [13] of the absorption line and ω_o is the mean optical resonance frequency. The oscillator strength of the $D1$ line of an alkali-metal atom corresponding to excitation of the $^2P_{1/2}$ state is $f \approx 1/3$ and the oscillator strength for the $D2$ line, corresponding excitation of the $^2P_{3/2}$ state, is $f \approx 2/3$. With these definitions the polarizability in Eq. (42) becomes

$$\vec{\alpha}_{\mu\nu}(\omega) = \frac{2r_e c^2 f}{\omega_o}\sum_k \frac{\mathbf{A}_{\mu k}\mathbf{A}_{k\nu}^\dagger}{\omega_{k\nu} - \omega - i\gamma_o}. \tag{46}$$

Now consider the polarizability of a coherent superposition state for the important 0-0 clock transition between an upper sublevel $|\alpha\rangle = |a0\rangle$ and a lower sublevel $|\beta\rangle = |b0\rangle$. Here the total angular momentum quantum numbers of the upper and lower states are $f = I + 1/2 = a$ and $f = I - 1/2 = b$; the azimuthal quantum numbers of both states are $m = 0$. The density matrix is

$$\rho = \frac{1}{2}(|\alpha\rangle\langle\alpha| + |\beta\rangle\langle\beta| + |\alpha\rangle\langle\beta|e^{-i\Omega t} + |\beta\rangle\langle\alpha|e^{i\Omega t}). \tag{47}$$

The clock frequency is

$$\Omega = \frac{E_\alpha - E_\beta}{\hbar}. \tag{48}$$

Combining Eqs. (47) and (46) in Eq. (41), we find

$$\langle\vec{\alpha}(\omega,t)\rangle = \frac{r_e c^2 f}{\omega_o}\sum_k \left[\frac{\mathbf{A}_{\alpha k}\mathbf{A}_{k\alpha}^\dagger + \mathbf{A}_{\beta k}\mathbf{A}_{k\alpha}^\dagger e^{-i\Omega t}}{\omega_{k\alpha} - \omega - i\gamma_o} \right.$$
$$\left. + \frac{\mathbf{A}_{\beta k}\mathbf{A}_{k\beta}^\dagger + \mathbf{A}_{\alpha k}\mathbf{A}_{k\beta}^\dagger e^{i\Omega t}}{\omega_{k\beta} - \omega - i\gamma_o} \right]. \tag{49}$$

For buffer-gas pressures exceeding a few hundred Torr, the pressure broadening of the optical absorption line is so large that $|\omega_{kl}| \ll \gamma_o$ for any pair of E_k and E_l of the excited state. In this limit, we can neglect the dependence of $\omega_{k\alpha}$ or $\omega_{k\beta}$ on k and write the frequency denominators of Eq. (49) as

$$\omega_{k\alpha} = \omega_o - \Omega/2, \quad \omega_{k\beta} = \omega_o + \Omega/2, \tag{50}$$

where ω_o is the mean frequency of the optical absorption line. Then the summation on k in Eq. (49) can be dropped by closure, and we can write

$$\langle\vec{\alpha}(\omega,t)\rangle = \alpha(\omega + \Omega/2)[\langle\alpha|\mathbf{A}\mathbf{A}^\dagger|\alpha\rangle + \langle\beta|\mathbf{A}\mathbf{A}^\dagger|\alpha\rangle e^{-i\Omega t}]$$
$$+ \alpha(\omega - \Omega/2)[\langle\beta|\mathbf{A}\mathbf{A}^\dagger|\beta\rangle + \langle\alpha|\mathbf{A}\mathbf{A}^\dagger|\beta\rangle e^{i\Omega t}]. \tag{51}$$

The coefficients $\alpha(\omega \pm \Omega/2)$ were defined by the second line of Eq. (18). The dimensionless operator $\mathbf{A}\mathbf{A}^\dagger$ for both the $D1$ line ($J = 1/2$) and the $D2$ line ($J = 3/2$) of alkali-metal atoms has a simple form [14]

$$\mathbf{A}\mathbf{A}^\dagger = \frac{\overleftrightarrow{\mathbf{I}}}{4} - \frac{(-1)^{J-S}}{[J]}\mathbf{S}\cdot\vec{\mathbf{s}}.\tag{52}$$

The unit dyadic is

$$\overleftrightarrow{\mathbf{I}} = \sum_k \mathbf{x}_k\mathbf{x}_k.\tag{53}$$

The projections of photon spin operator on the Cartesian axes $k = 1, 2, 3$ are

$$\vec{s}_k = \sum_{lm} \frac{\epsilon_{klm}\mathbf{x}_l\mathbf{x}_m}{i}.\tag{54}$$

Here the antisymmetric unit tensor $\epsilon_{klm} = \mathbf{x}_k \cdot (\mathbf{x}_l \times \mathbf{x}_m)$ is zero if any two of the indices klm are equal; it has the value $+1$ if klm is an even permutation of 123 and it is -1 if the permutation is odd.

The projections in Eq. (54) satisfy the usual commutation relations for spin operators,

$$[\vec{s}_k, \vec{s}_l] = i\sum_m \epsilon_{klm}\vec{s}_m.\tag{55}$$

One can also verify that $\Sigma_k \vec{s}_k \cdot \vec{s}_k = S(S+1)\overleftrightarrow{\mathbf{I}}$, with $S = 1$. The true photon spin of Eq. (5) is

$$\mathbf{s} = \sum_k \mathbf{x}_k(\mathbf{e}^* \cdot \vec{s}_k \cdot \mathbf{e}).\tag{56}$$

We can choose the phases of $|\alpha\rangle$ and $|\beta\rangle$ such that the matrix elements needed to evaluate Eq. (51) are

$$\langle\beta|\mathbf{S}|\alpha\rangle = \langle\alpha|\mathbf{S}|\beta\rangle = \frac{\mathbf{z}}{2},\tag{57}$$

from which we conclude that the expectation value of the electron spin for the superposition state, Eq. (47), is

$$\langle\mathbf{S}\rangle = \mathrm{Tr}[\rho\mathbf{S}] = \frac{1}{2}\mathbf{z}\cos\Omega t.\tag{58}$$

Using Eqs. (57) and (52) to evaluate Eq. (51), we find

$$\langle\vec{\alpha}(\omega,t)\rangle = \frac{\alpha(\omega+\Omega/2)}{4}\left[\overleftrightarrow{\mathbf{I}} - \frac{2(-1)^{J-S}}{[J]}\vec{s}_z e^{-i\Omega t}\right]$$
$$+ \frac{\alpha(\omega-\Omega/2)}{4}\left[\overleftrightarrow{\mathbf{I}} - \frac{2(-1)^{J-S}}{[J]}\vec{s}_z e^{i\Omega t}\right].\tag{59}$$

For optical pumping with circularly polarized light, it is often more convenient to use the spherical basis vectors $\boldsymbol{\xi}_m$ rather than the Cartesian basis vectors $\mathbf{x}_i$. The spherical basis vectors are given by

$$\boldsymbol{\xi}_{\pm 1} = \frac{\mathbf{x}_1 \pm i\mathbf{x}_2}{\mp\sqrt{2}} = \frac{\mathbf{x} \pm i\mathbf{y}}{\mp\sqrt{2}}, \quad \boldsymbol{\xi}_0 = \mathbf{x}_3 = \mathbf{z}.\tag{60}$$

In terms of these two bases, the longitudinal component of the photon spin operator, Eq. (54), can be written as

$$\vec{s}_z = \frac{1}{i}(\mathbf{x}\mathbf{y} - \mathbf{y}\mathbf{x}) = \boldsymbol{\xi}_1\boldsymbol{\xi}_1^* - \boldsymbol{\xi}_{-1}\boldsymbol{\xi}_{-1}^*.\tag{61}$$

Using Eq. (61) to take the matrix elements of Eq. (59) for light of polarization $\boldsymbol{\xi}_{-1}$ (photon spin antiparallel to the z axis), the polarizability matrix element for $D1$ light with $J = 1/2$ becomes

$$\boldsymbol{\xi}_{-1}^* \cdot \langle\vec{\alpha}(\omega,t)\rangle \cdot \boldsymbol{\xi}_{-1} = \frac{\alpha(\omega+\Omega/2)}{4}(1 + e^{-i\Omega t})$$
$$+ \frac{\alpha(\omega-\Omega/2)}{4}(1 + e^{i\Omega t}).\tag{62}$$

This is precisely the same form as Eq. (23), the polarizability for a classical dipole antenna excited by light polarized along the x axis. So Figs. 3–6 can also be interpreted as the response of an alkali-metal atom in the pure superposition state (47) to modulated, negative-helicity light, with the polarization vector $\mathbf{e} = \boldsymbol{\xi}_{-1}$ and $\mathbf{s} = -\mathbf{z}$. The atom has no response at times when $2\mathbf{s}\cdot\langle\mathbf{S}\rangle = 1$, since it cannot conserve angular momentum if it absorbs light at those times.

For $D2$ light with $J = 3/2$, the matrix element is

$$\boldsymbol{\xi}_{-1}^* \cdot \langle\vec{\alpha}(\omega,t)\rangle \cdot \boldsymbol{\xi}_{-1} = \frac{\alpha(\omega+\Omega/2)}{4}\left(1 - \frac{e^{-i\Omega t}}{2}\right)$$
$$+ \frac{\alpha(\omega-\Omega/2)}{4}\left(1 - \frac{e^{i\Omega t}}{2}\right).\tag{63}$$

As mentioned in the Introduction, there is no possibility of getting a true dark state for $D2$ pumping, since the factors $(1 - e^{\pm i\Omega t}/2)$ of Eq. (63) have no nulls as a function of time. At best, one can get "dim" states. The superiority of circularly polarized $D1$ light over $D2$ light for the pumping of alkali-metal atoms has long been known [15] and has recently been demonstrated experimentally for CPT pumping [16].

IV. OPTIMAL CPT WAVE FORMS

In Figs. 3–6 we showed detailed examples of how the saturation of CPT signals depends on the broadening of the optical absorption lines. For alkali-metal atoms, the broadening is mainly due to the buffer gas that is used to prevent the atoms from diffusing to the cell walls too quickly. In this section, we show that for systems such as the linear antenna of Sec. II or such as alkali-metal atoms in the 0-0 superposition state of Eq. (47), there is an optimal, pressure-dependent modulation format that minimizes the required optical power and maximizes the resonance saturation.

We write the electric field of the light as the product of a carrier wave of frequency ω_o and time-independent amplitude K and a periodic, dimensionless envelope $\mathcal{E}$:

$$E = Ke^{-i\omega_o t}\mathcal{E}.\tag{64}$$

The envelope is the Fourier series

$$\mathcal{E} = \sum_\kappa \varepsilon^{(\kappa)}e^{-i\kappa\Omega t}.\tag{65}$$

As can be seen from Eq. (28), the time-averaged power absorbed by bright or dark waves depends on the constructive or destructive interference of sideband amplitudes spaced by

Ω in the frequency domain. We therefore include sidebands spaced by Ω in Eq. (65), rather than those spaced by $\Omega/2$ in the analogous expansion of Eq. (24). In Secs. IV and V, Greek summation indices such as κ or λ will always denote positive and negative half-integers—for example, $\kappa = \pm 1/2, \pm 3/2, \pm 5/2, \ldots$—while Latin summation indices such as q will always denote positive and negative integers and 0. Because of the half-integer summation indices κ, the periodicity of Eq. (65) is

$$\mathcal{E}(t + qT) = (-1)^q \mathcal{E}(t). \qquad (66)$$

Using Eqs. (18) and (65) to evaluate α'' in Eq. (28), we write the mean power absorbed by the antenna (or atom) as

$$P = \frac{2\mathcal{A}}{\gamma_o^2} \sum_\kappa \frac{|\varepsilon^{(\kappa)} + \varepsilon^{(\kappa+1)}|^2}{2 + (\kappa + 1/2)^2 r^2}, \qquad (67)$$

where we define the *resolution parameter* by

$$r = \frac{\Omega\sqrt{2}}{\gamma_o} \qquad (68)$$

and $\mathcal{A}$ was defined in Eq. (33). The mean absorbed power (67) will vanish if the sideband amplitudes $\varepsilon^{(\kappa)}$ have alternating signs and equal magnitudes. We therefore define the *ideal dark wave* with amplitudes that alternate between i and $-i$ by

$$\varepsilon_d^{(\kappa)} = e^{-i\kappa\pi}. \qquad (69)$$

The envelope of Eq. (65) defined by Eq. (69) is

$$\mathcal{E}_d(t) = \sum_\kappa e^{-i\kappa\Omega(t+T/2)} = Te^{-i\Omega(t+T/2)/2} \sum_\kappa \delta(t - \kappa T). \quad (70)$$

The ideal dark wave, Eq. (70), is not absorbed because the δ-function pulses reach the antenna or the atoms when the polarizabilities in Eqs. (23) and (62) are exactly zero.

If we delay the envelope (70) by $T/2$, we get the envelope of the *ideal bright wave*,

$$\mathcal{E}_b(t) = \mathcal{E}_d(t - T/2) = \sum_\kappa e^{-i\kappa\Omega t} = Te^{-i\Omega t/2} \sum_q \delta(t - qT). \qquad (71)$$

The sideband coefficients of the bright wave are evidently

$$\varepsilon_b^{(\kappa)} = 1 = e^{i\kappa\pi}\varepsilon_d^{(\kappa)}. \qquad (72)$$

Using the amplitudes of Eq. (72) in Eq. (67), we find that the power absorbed from the ideal bright wave is

$$P_b = \frac{8\mathcal{A}}{\gamma_o^2} \sum_q \frac{1}{2 + q^2 r^2} = 2\pi r_e c f[\coth(\pi\gamma_o/\Omega)]\frac{dS}{d\nu}, \quad (73)$$

where the sum in the first line of Eq. (73) extends over the integers $q = 0, \pm 1, \pm 2, \ldots$. The time-independent amplitude K is related to the spectral density $dS/d\nu$ of power carried by the light (units: erg s^{-1} cm^{-2} Hz^{-1}) by

$$cK^2 = \Omega\frac{dS}{d\nu}. \qquad (74)$$

The sum in Eq. (73) can be evaluated from the well-known partial-fraction expansion [17] $\cot x = \Sigma_q x/(x^2 - q^2\pi^2)$.

The waves given in Eqs. (70) and (71) are impractical idealizations, but they are a good introduction to *optimal CPT waves* which can be produced with practical modulation schemes. We assume that the sideband amplitudes $\varepsilon_b^{(\kappa)}$ of the optimal bright wave depend on κ and are normalized to unity,

$$\sum_\kappa |\varepsilon_b^{(\kappa)}|^2 = 1. \qquad (75)$$

The mean absorbed power (67) from the optimal bright wave can be written in matrix format

$$P_b = P_0 \sum_{\kappa\lambda} \varepsilon_b^{(\kappa)*} \Pi_{\kappa\lambda} \varepsilon_b^{(\lambda)}, \qquad (76)$$

where the characteristic power is

$$P_0 = \frac{r_e c^2 f K^2}{2\gamma_o} = \frac{\pi r_e c f S}{\gamma_o}. \qquad (77)$$

Here $S = cK^2/2\pi$ is the flux (units: erg s^{-1} cm^{-2}) of the wave. The nonzero elements of the power-absorption matrix Π of Eq. (76) are

$$\Pi_{\kappa,\kappa\pm 1} = \frac{2}{2 + (\kappa \pm 1/2)^2 r^2} \qquad (78)$$

and

$$\Pi_\kappa = \Pi_{\kappa,\kappa+1} + \Pi_{\kappa,\kappa-1} = \frac{2}{2 + (\kappa + 1/2)^2 r^2} + \frac{2}{2 + (\kappa - 1/2)^2 r^2}. \qquad (79)$$

In accordance with Eqs. (72) and (76), the mean power absorbed by the optimal dark wave is

$$P_d = P_0 \sum_{jk} \varepsilon_d^{(\kappa)*} \Pi_{\kappa\lambda} \varepsilon_d^{(\lambda)} = P_0 \sum_{\kappa\lambda} \varepsilon_b^{(\kappa)*} \Pi_{\kappa\lambda} \lambda_b^{(\lambda)} (-1)^{\kappa-\lambda}. \qquad (80)$$

The difference between the powers absorbed by the optimal bright and dark waves is

$$P_b - P_d = P_0 \sum_{jk} \varepsilon_b^{(\kappa)*} \Delta_{\kappa\lambda} \varepsilon_b^{(\lambda)} = P_0 \langle \varepsilon_b | \Delta | \varepsilon_b \rangle. \qquad (81)$$

The only nonzero elements of the power-difference matrix are

$$\Delta_{\kappa,\kappa\pm 1} = 2\Pi_{\kappa,\kappa\pm 1} = \frac{4}{2 + (\kappa \pm 1/2)^2 r^2}. \qquad (82)$$

In analogy to Eq. (81), we find that the sum of the powers absorbed by the optimal bright and dark waves is

$$P_b + P_d = P_0 \sum_{\kappa\lambda} \varepsilon_b^{(\kappa)*} \Sigma_{\kappa\lambda} \varepsilon_b^{(\lambda)} = P_0 \langle \varepsilon_b | \Sigma | \varepsilon_b \rangle. \qquad (83)$$

The only nonzero elements of the power-sum matrix are

$$\Sigma_{\kappa\kappa} = 2\Pi_{\kappa\kappa} = \frac{4}{2 + (\kappa + 1/2)^2 r^2} + \frac{4}{2 + (\kappa - 1/2)^2 r^2}. \quad (84)$$

The saturation (34) of the optimal wave is therefore

$$\mathcal{S} = \frac{P_b - P_d}{P_b + P_d} = \frac{\langle \varepsilon_b | \Delta | \varepsilon_b \rangle}{\langle \varepsilon_b | \Sigma | \varepsilon_b \rangle}. \quad (85)$$

One might think that the criterion for the optimal wave would be the wave for which the saturation (85) reaches its maximum value $\mathcal{S}=1$. But we have already found the solution that maximizes $\mathcal{S}$: namely, the ideal bright wave in Eq. (71). Such waves are not practical to produce; nor would they be practical in use, since essentially all of the light would be off resonance and the fraction of power absorbed from the ideal bright wave would be vanishingly small. CPT resonances observed by changes in laterally scattered atomic fluorescence would be overwhelmed by instrumentally scattered, off-resonant light. CPT resonances observed as changes in the transmitted light would also be vanishingly small. A practical criterion for the optimal wave is the wave that maximizes the power difference of Eq. (81), the numerator of Eq. (85).

Since the power difference [Eq. (77)] is the expectation value of the Hermitian power-difference operator Δ, finding the optimum wave consists of finding the solution to the eigenvalue equation

$$\Delta | \varepsilon_n \rangle = \delta_n | \varepsilon_n \rangle, \quad (86)$$

with the largest eigenvalue $\delta_b \geqslant \delta_n$ for all eigenvalues δ_n. The Fourier amplitudes of the optimal bright wave are the eigenvectors $\varepsilon_b^{(\kappa)}$. We set the phase of the amplitudes by taking them to be real with $\varepsilon_b^{(1/2)} > 0$. Since Δ is Hermitian, all of its eigenvalues δ_n are real. In terms of the amplitudes $\langle \kappa | \varepsilon_n \rangle = \varepsilon_n^{(\kappa)}$ of $| \varepsilon_n \rangle$, Eq. (86) is equivalent to the infinite set of coupled equations

$$\frac{4\varepsilon_n^{(\kappa+1)}}{2 + (\kappa + 1/2)^2 r^2} + \frac{4\varepsilon_n^{(\kappa-1)}}{2 + (\kappa - 1/2)^2 r^2} = \delta_n \varepsilon_n^{(\kappa)}. \quad (87)$$

There are useful symmetries to the solutions of Eq. (87). First, since the coefficients of the coupled equations in Eq. (87) are real, the eigenvector amplitudes $\varepsilon_n^{(\kappa)}$ can be chosen to be real.

Let $| \varepsilon_n \rangle$ be an eigenvector of Eq. (87) with eigenvalue δ_n. Consider the *reflected* vector $\sigma | \varepsilon_n \rangle$ with the amplitudes

$$\langle \kappa | \sigma | \varepsilon_n \rangle = \langle -\kappa | \varepsilon_n \rangle = \varepsilon_n^{(-\kappa)}. \quad (88)$$

Substituting Eq. (88) into Eq. (87) we see that $\Delta \sigma | \varepsilon_n \rangle = \delta_n \sigma | \varepsilon_n \rangle$, so the reflected vector $\sigma | \varepsilon_n \rangle$ is also an eigenvector of Δ with the same eigenvalue δ_n as $| \varepsilon_n \rangle$. If there are no degenerates, we conclude that $\sigma | \varepsilon_n \rangle = \lambda_n | \varepsilon_n \rangle$, where λ_n is an eigenvalue of σ. Two reflections cancel, so $\sigma^2 = 1$ and $\lambda_n = \pm 1$. We conclude that a nondegenerate eigenvector $| \varepsilon_n \rangle$, must be even or odd under the reflection operation $\sigma | \varepsilon_n \rangle = \pm | \varepsilon_n \rangle$. The reflection operator commutes with the operators Δ and Σ — that is, $\sigma\Delta - \Delta\sigma = 0$ and $\sigma\Sigma - \Sigma\sigma = 0$.

The bright wave is even, and its envelope is given explicitly by

$$\mathcal{E}_b(t) = \sum_\kappa \varepsilon_b^{(\kappa)} e^{-i\kappa\Omega t}, \quad (89)$$

where the real amplitudes have the reflection symmetry $\varepsilon_b^{(-\kappa)} = \varepsilon_b^{(\kappa)}$. The same symmetries imply that the envelope is an even function of time, so

$$\mathcal{E}_b(-t) = \mathcal{E}_b(t). \quad (90)$$

Evaluating the envelope in Eq. (89) at $t = T/2$ we find that

$$\mathcal{E}_b(T/2) = \sum_j \varepsilon_b^{(\kappa)} e^{-i\kappa\pi} = 0. \quad (91)$$

The sum in Eq. (91) is zero because $e^{i\kappa\pi} = -e^{-i\kappa\pi}$ for the half-integer summation indices κ and because $\varepsilon_b^{(\kappa)} = \varepsilon_b^{(-\kappa)}$. From Eqs. (66) and (91), we see that the envelope $\mathcal{E}_b$ will have zero crossings at $T/2 + qT$, where $q = 0, \pm 1, \pm 2, \dots$ is any integer.

Turning now to a second symmetry of Eq. (87), we define the antiphase wave $\tau | \varepsilon_n \rangle$ corresponding to $| \varepsilon_n \rangle$ by the elements

$$\langle \kappa | \tau | \varepsilon_n \rangle = e^{-i\kappa\pi} \langle \kappa | \varepsilon_n \rangle = e^{-i\kappa\pi} \varepsilon_n^{(\kappa)}. \quad (92)$$

Substituting Eq. (92) into Eq. (87) we see that $\Delta \tau | \varepsilon \rangle = -\delta_n \tau | \varepsilon_n \rangle$, so $\tau | \varepsilon_n \rangle$ is also an eigenvector of Δ with eigenvalue $-\delta_n$. The antiphase operator τ anticommutes with Δ — that is, $\tau\Delta + \Delta\tau = 0$. It commutes with Σ — that is, $\tau\Sigma - \Sigma\tau = 0$. Note that $\tau^2 = -1$.

The antiphase operator shifts the time origin of envelopes by $-T/2$,

$$\tau\mathcal{E}(t) = \mathcal{E}(t + T/2). \quad (93)$$

Applying the antiphase operator τ to a bright wave produces the corresponding dark wave, $\varepsilon_d^{(\kappa)} = e^{-i\kappa\pi} \varepsilon_b^{(\kappa)}$.

The eigenvalue spectrum of Δ is plotted as a function of γ_o/Ω in the upper panel of Fig. 7, and the saturation $\mathcal{S}$ of Eq. (85) is plotted on the same horizontal scale in the lower panel. For low buffer-gas pressures, the bright wave corresponds to the eigenvalue $\delta_b = 2$, and the corresponding envelope has only two nonzero sidebands with $\kappa = \pm 1/2$. The corresponding envelopes are

$$\mathcal{E}_b(t) = \sqrt{2}\cos(\Omega t/2),$$

$$\mathcal{E}_d(t) = -\sqrt{2}\sin(\Omega t/2). \quad (94)$$

The saturation is $\mathcal{S}=1$ for the low-pressure limit. The antiphase, dark wave has the only other nonzero eigenvalue $\delta_d = -2$. At low pressure, all eigenvalues except those of the bright and dark waves are zero. These correspond to waves for which the resonant sidebands $\varepsilon_n^{\pm 1/2}$ have zero amplitude. All of these high-resolution results can be verified with a perturbation-theory solution of Eq. (87).

In the high-pressure limit with $r \ll 1$, large numbers of nonzero eigenvalues evolve from those that were zero in the low-pressure limit. The eigenvalue of the bright state approaches the limit $\delta_b = 4$ as $\gamma_o/\Omega \to \infty$. Because of the broad optical absorption linewidth, the bright wave has many sidebands. For the $\gamma_o/\Omega \to \infty$ limit, one can verify that the sideband amplitudes approach the limiting value
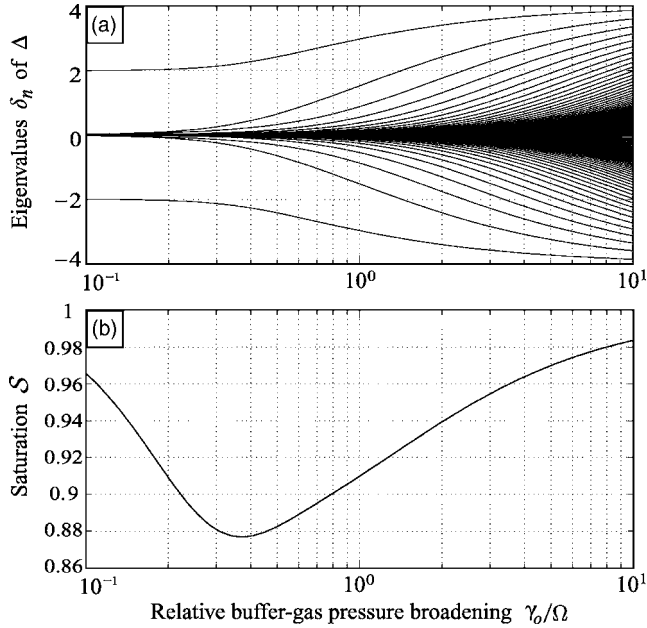
FIG. 7. (a) Eigenvalue spectrum of the power-difference matrix Δ of Eq. (77) and (b) the saturation $\mathcal{S}$ of Eq. (85) for the optimal CPT wave, Eq. (89), plotted versus the buffer-gas pressure γ_o divided by the hyperfine splitting Ω. There is a quasicontinuum of eigenvalues δ_n with values close to zero, corresponding to waves with mostly off-resonant sidebands. The eigenvalue δ_b of the bright wave is the topmost line in panel (a). For the low-pressure limit $(r \to \infty)$ we see that $\delta_b \to 2$. In the high-pressure case $(r \to 0)$ we see that $\delta_b \to 4$. In both limits $\mathcal{S} \to 1$, the saturation approaches its maximum possible value.

$$\varepsilon_b^{(\kappa)} \approx \left(\frac{r}{\pi}\right)^{1/4} e^{-r\kappa^2/2}, \qquad (95)$$

where $r = \sqrt{2}\Omega/\gamma_o$. Substituting the amplitudes of Eq. (95) into Eq. (65) we find the low-resolution approximation to the bright-wave envelope,

$$\mathcal{E}_b = \left(\frac{4\pi}{r}\right)^{1/4} \sum_q (-1)^q e^{-\Omega^2(t - qT)^2/(2r)}. \qquad (96)$$

The low-resolution envelope is a train of well-resolved Gaussian functions of alternating sign. One could imagine generating such a wave by passing a monochromatic laser beam with the frequency ω_o through a phase modulator with the purely imaginary modulation index

$$m = \frac{i}{r} = \frac{i\gamma_o}{\Omega\sqrt{2}}. \qquad (97)$$

Optimal wave forms for low- and high-pressure p are shown in Fig. 8. The three pairs of plots represent three different pressure scenarios: low pressure at the top, where $\gamma_o \ll \Omega$; intermediate pressure in the middle, where $\gamma_o \approx \Omega$; and very high pressure at the bottom, where $\gamma_o \gg \Omega$. The frequency-domain plots on the left show the sideband amplitudes of the optimal bright wave and the atomic (or antenna) absorption profile. On the right the optimal bright wave envelope is plotted as a function of time. As the pressure in-
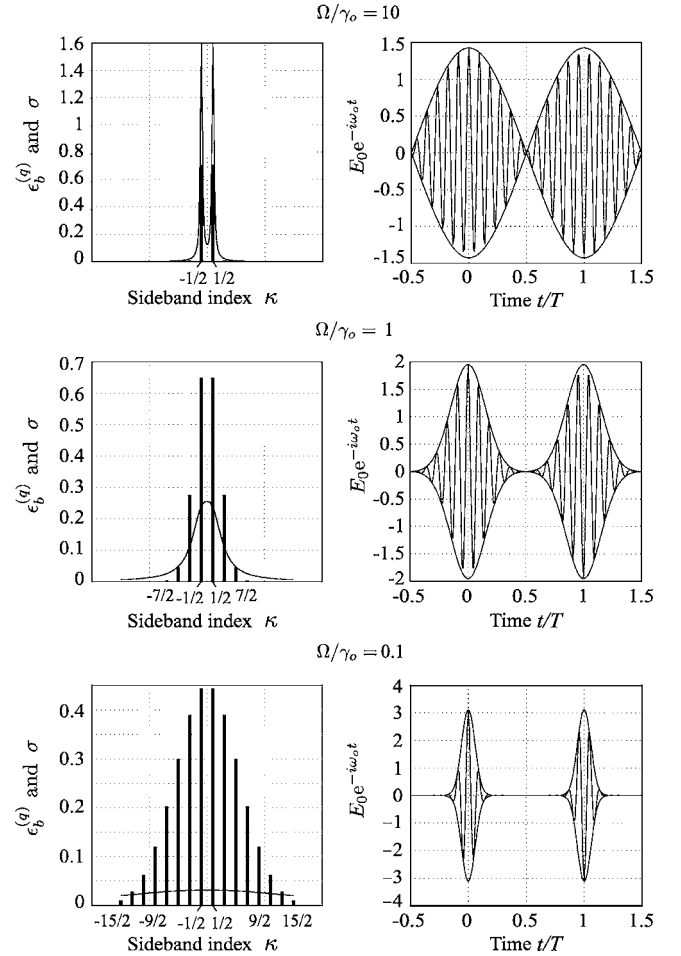

FIG. 8. Optimal bright waves in the frequency domain (left) and time domain (right). The sideband frequencies are $\omega_\kappa = \omega_o + \kappa\Omega$, where $\kappa = \pm 1/2, \pm 3/2, \dots$. Also shown in the left panel are the pressure-broadened optical absorption cross sections. The wave of the top panels is for low buffer-gas pressure where the atoms have well-resolved hyperfine structure $\Omega/\gamma_o = 10$. The wave has two strong frequencies, spaced by the resonance frequency Ω. Other sidebands have negligible amplitudes. The wave of middle panel is for intermediate pressure, with $\Omega/\gamma_o = 1$, just enough for the hyperfine splitting to be unresolved. The wave has several strong frequencies, and the time-domain envelopes are narrowed. The wave of the bottom panel is for high pressure, with $\Omega/\gamma_o = 0.1$, where the optical line broadening is much greater than the hyperfine splitting. The optimal wave has many frequencies, and the time-domain envelopes are very narrow.

creases, the number of sidebands needed for the optimal wave increases with the square root of the pressure. The temporal width of the envelope pulses is inversely proportional to the square root of the pressure.

V. OPTIMUM PUSH-PULL WAVES

The optimal CPT waves of the previous section must serve two purposes: (a) the saturation $\mathcal{S}$ of Eq. (85) must be as close to unity as possible to give strong resonance signals, and (b) the wave must efficiently pump the atoms into the 0-0 superposition state of Eq. (47) by "burning out" other

states which absorb light more strongly. Unfortunately, except for the impractical "ideal dark wave" of Eq. (70), the 0-0 superposition state absorbs a small, but nonzero amount of optical power, while the end states $\rho = |a, \pm a\rangle\langle a, \pm a|$ for photon spin $s_z = \pm 1$ absorb no light at all, since their polarizabilities are identically zero. Therefore pumping with modulated light of fixed circular polarization eventually transfers all of the atoms into the end states [10], the stable dark states for light of fixed circular polarization. To avoid this "trapping" the intensity of the CPT pumping light must be limited, so that collisional damping prevents all of the atoms from accumulating in the end state. This severely limits the size of the CPT resonance signals.

By using $D1$ light with modulated circular polarization or *push-pull pumping*, Jau *et al.* [9] have shown that it is possible to make the 0-0 state the only dark state of the system. A simple way to make an optimum push-pull wave is to split an optimal CPT wave (89) into two waves with an optical beam splitter to reverse the polarization of one of the waves and advance or retard it in time by $T/2$ before recombining it with the other wave. The superposed waves will pump the atoms into the 0-0 state.

Let the two waves have orthogonal circular polarization vectors $\boldsymbol{\xi}_{\pm 1}$ defined by Eq. (60). The photon spins corresponding to these two waves are

$$\mathbf{s}_{\pm 1} = i\boldsymbol{\xi}_{\pm 1} \times \boldsymbol{\xi}_{\pm 1}^* = \pm \mathbf{z}. \tag{98}$$

Noting that $\mathcal{E}_b(t+T/2) = \mathcal{E}_d(t)$ we see that an optimum optimum push-pull wave is

$$\mathbf{E} = \frac{e^{-i\omega_o t}}{\sqrt{2}} \{\boldsymbol{\xi}_{-1}\mathcal{E}_b(t) - \boldsymbol{\xi}_1\mathcal{E}_d(t)e^{-i\omega_o T/2}\}$$

$$= \frac{e^{-i\omega_o t}}{\sqrt{2}} \sum_{\kappa_+} \varepsilon_b^{(\kappa_+)} e^{-i\kappa_+\Omega t}\{\boldsymbol{\xi}_{-1} - \boldsymbol{\xi}_1 e^{-i2\phi_+}\}$$

$$+ \frac{e^{-i\omega_o t}}{\sqrt{2}} \sum_{\kappa_-} \varepsilon_b^{(\kappa_-)} e^{-i\kappa_-\Omega t}\{\boldsymbol{\xi}_{-1} - \boldsymbol{\xi}_1 e^{-i2\phi_-}\}$$

$$= e^{-i\omega_o(t+T/4)}\{\mathcal{E}_+(t)\mathbf{e}_+ + \mathcal{E}_-(t)\mathbf{e}_-\}. \tag{99}$$

As indicated in Eq. (99) it is convenient to partition the half-integer summation indices $\kappa = \pm 1/2, \pm 3/2, \pm 5/2$ into the two subsets $\kappa_\pm = \pm 1/2 + 2q$, where $q = 0, \pm 1, \pm 2, \ldots$ is any integer. We note that $e^{-i\kappa_\pm\pi} = e^{\mp i\pi/2}$. The phases are

$$\phi_\pm = (\omega_o T \pm \pi)/4. \tag{100}$$

The linearly polarized unit vectors are

$$\mathbf{e}_\pm = \mathbf{x}\cos\phi_\pm + \mathbf{y}\sin\phi_\pm. \tag{101}$$

These vectors are at right angles to each other. The dot and cross products are

$$\mathbf{e}_- \cdot \mathbf{e}_+ = 0, \quad \mathbf{e}_- \times \mathbf{e}_+ = \mathbf{z}. \tag{102}$$

The push-pull envelope functions are

$$\mathcal{E}_\pm(t) = e^{\mp i\pi/4}\sum_{j_\pm} \varepsilon_b^{(\kappa_\pm)} e^{-i\kappa_\pm\Omega t}. \tag{103}$$

Since the summation indices $\kappa_\pm$ are equal and opposite and since $\varepsilon_b^{(-\kappa)} = \varepsilon_b^{(\kappa)}$, the envelope functions are complex conjugates of each other, $\mathcal{E}_+(t) = \mathcal{E}_-^*(t)$.

From inspection of Eq. (100) we find that

$$\mathcal{E}_\pm(t - qT/2) = (\pm i)^q\mathcal{E}_\pm(t), \tag{104}$$

where $q = 0, \pm 1, \pm 2, \ldots$ is any integer. From inspection of the push-pull envelopes in Eq. (103) we find that we can write the envelopes for the optimum CPT bright and dark waves as

$$\mathcal{E}_b(t) = e^{i\pi/4}\mathcal{E}_+(t) + e^{-i\pi/4}\mathcal{E}_-(t) \tag{105}$$

and

$$\mathcal{E}_d(t) = e^{-i\pi/4}\mathcal{E}_+(t) + e^{i\pi/4}\mathcal{E}_-(t). \tag{106}$$

Conversely, we can write

$$\mathcal{E}_\pm(t) = \frac{e^{\mp i\pi/4}\mathcal{E}_b(t) + e^{\pm i\pi/4}\mathcal{E}_d(t)}{2}$$

$$= \frac{e^{\mp i\pi/4}\mathcal{E}_b(t) + e^{\pm i\pi/4}\mathcal{E}_b(t + T/2)}{2}. \tag{107}$$

As can be seen from the first line of Eq. (99), the optimum push-pull wave consists of two pulse trains of opposite circular polarization. The trains are interleaved so the intensity of right-circularly polarized light is maximum when the intensity of left-circularly polarized light is minimum. The pulse repetition frequency for each sense of circular polarization is Ω.

Alternately, the last line of Eq. (99) shows that the optimum push-pull wave can be thought of as overlapping pulse trains of orthogonal linear polarizations $\mathbf{e}_-$ and $\mathbf{e}_+$. The repetition frequency for the linearly polarized pulses is 2Ω since the sidebands in the envelopes of Eq. (103) are spaced by 2Ω. The peaks of the pulse envelopes coincide, and the phases are such that the combined waves have pure circular polarization at their peaks. The sign of the circular polarization alternates from pulse to pulse. In the frequency domain, the polarizations of the sidebands alternate between the orthogonal linear polarizations $\mathbf{e}_-$ and $\mathbf{e}_+$.

In the high-resolution (low-pressure) limit, we can use Eq. (94) with Eq. (107) to show that

$$\mathcal{E}_\pm(t) = \frac{e^{\mp i\Omega(t+T/4)/2}}{\sqrt{2}}. \tag{108}$$

The optimal push-pull wave of Eq. (99) is then

$$\mathbf{E} = e^{-i\omega_o t}\{\boldsymbol{\xi}_{-1}\cos(\Omega t/2) + \boldsymbol{\xi}_1\cos(\Omega t/2)e^{-i\omega_o T/2}\}$$

$$= \frac{1}{2}\{\mathbf{e}_+ e^{-i[\omega_o+\Omega/2](t+T/4)} + \mathbf{e}_- e^{-i[\omega_o-\Omega/2](t+T/4)}\}. \tag{109}$$

Optimum push-pull waves and their corresponding spectra are plotted in Fig. 9. The sideband frequencies are $\omega_\kappa = \omega_o + \kappa\Omega$, where the sideband indices are $\kappa = \pm 1/2, \pm 3/2, \ldots$. Also shown in the left panels are the
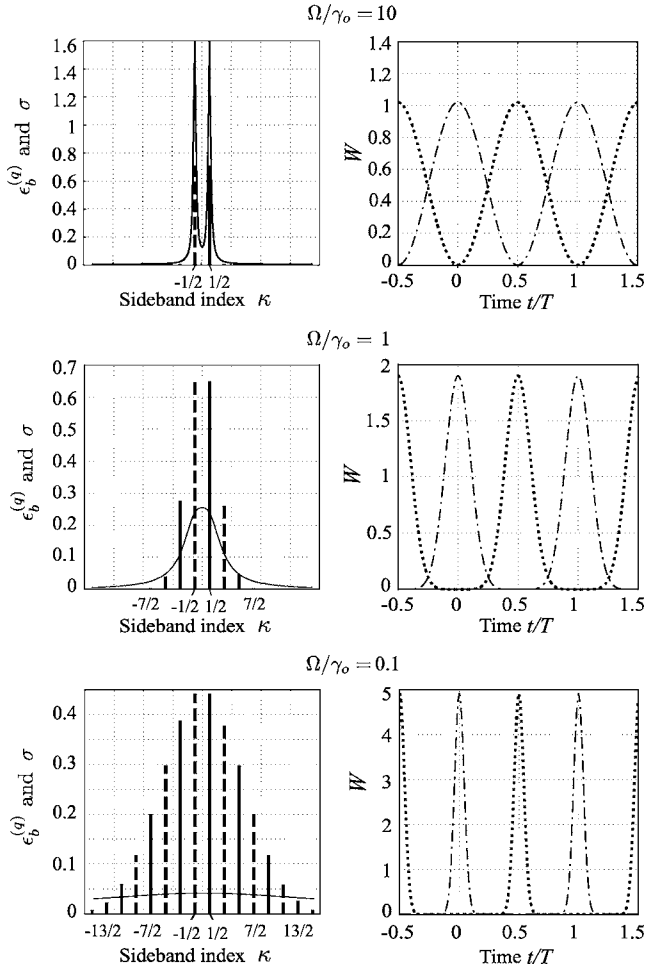
FIG. 9. Optimal bright push-pull waves in the frequency domain (left) and time domain (right). Sideband amplitudes with the linear polarization $\mathbf{e}_+$ of Eq. (99) are shown as solid lines in the left panels, and amplitudes with the orthogonal linear polarization $\mathbf{e}_-$ are shown as dashed lines. The right panels show the intensity $W = |\mathcal{E}_b|^2$ of light of circular polarization $\boldsymbol{\xi}_{-1}$ (dotted line) and the intensity $W = |\mathcal{E}_d|^2$ of light of the orthogonal circular polarization $\boldsymbol{\xi}_1$ (dash-dotted line) from the optimal push-pull wave of Eq. (99).
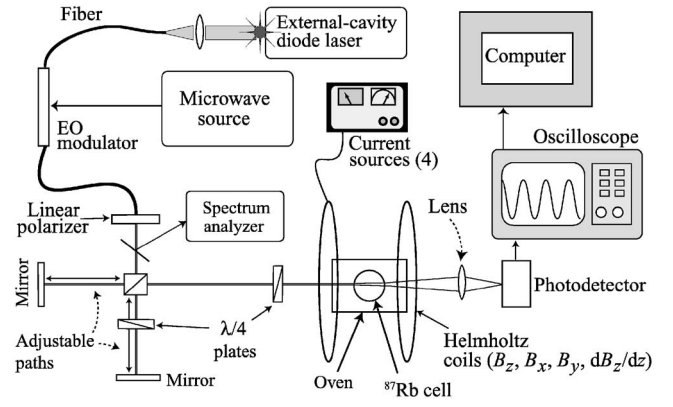

FIG. 10. Schematic diagram of the experimental apparatus.

ing linear polarization. In the time domain, the light consists of well resolved pulses of alternating circular polarization.

According to the first line of Eq. (109) we can think of the optimum push-pull wave as the superposition of two amplitude-modulated waves of opposite circular polarizations $\boldsymbol{\xi}_{\pm 1}$, both having the carrier frequency ω_o. Alternately, according to the second line of Eq. (109), we can think of the optimal push-pull wave as two monochromatic waves of frequencies $\omega_o \pm \Omega/2$ and of orthogonal linear polarizations $\mathbf{e}_\pm$. Zanon *et al.* [11] show that one can mode-lock two monochromatic lasers with orthogonal linear polarizations, such that their frequencies differ by Ω and are resonant for excitation from the upper and lower sublevels of the superposition state (47). They describe this modulation as "lin-$\perp$-lin." Of course, "lin-$\perp$-lin" waves can also be generated with AM light from a single laser, as discussed above and as demonstrated by Jau *et al.* [9]. For higher pressures, where the optimal push-pull waves require many frequency components, modulation with time delays and circular polarization reversals may be more practical, although it would also be possible to simultaneously amplitude-modulate lasers of orthogonal linear-polarizations and with carrier frequencies separated by Ω in a "lin-$\perp$-lin" pumping scheme to make the optimal envelopes $\mathcal{E}_\pm$ of Eq. (99).

VI. EXPERIMENT

For experimental validation, push-pull CPT signals with both FM and AM light were examined using cells of varying buffer-gas pressure. The experimental arrangement is shown in Fig. 10. The laser beam, functioning both as a pump and a probe beam, was generated by a Toptica external cavity diode laser centered on the $D1$ line of Rb (795 nm). Different modulators provided frequency and amplitude modulation. A single LiNbO$_3$ electro-optic crystal generated FM light, and the AM light was generated by a modulator that is described below.

In the theoretical section of this paper, we found it convenient to discuss both FM and AM light in terms of a generalized phase modulator, for which the modulation index m could be an arbitrary complex number. CPT signals for FM and AM light were modeled with purely real and purely imaginary values of m in Sec. II. In our experiments, AM

pressure-broadened optical absorption cross sections. The wave of the top panels is for low buffer-gas pressure where the atoms have well-resolved hyperfine structure $\Omega/\gamma_o = 10$. The wave has two strong frequencies, spaced by the resonance frequency Ω and of orthogonal linear polarizations. Other sidebands have negligible amplitudes. There is substantial overlap in time of the pulses of alternating circular polarization, so the polarization changes smoothly from circular to elliptical to linear, etc. The wave of middle panel is for intermediate pressure, with $\Omega/\gamma_o = 1$, just enough for the hyperfine splitting to be unresolved. The wave has several sidebands, of alternating linear polarization. There is little overlap in time of the pulses of alternating circular polarization, so the polarization changes more abruptly between relatively pure states of circular polarization. The wave of the bottom panel is for high pressure, with $\Omega/\gamma_o = 0.1$, where the optical line broadening is much greater than the hyperfine splitting. The optimal wave has many sidebands of alternat-

light was produced with a commercial Mach-Zehnder modulator. A Mach-Zehnder modulator works by splitting the light into two beams with real, positive electric-field amplitudes K_1 and K_2, with unbiased phases θ_1 and θ_2, and with electrically adjustable bias phases $\pm\phi$. The microwave modulation voltage introduces equal and opposite phase retardations $m\cos(\Omega\{t-t_0\}/2)$ to the two beams, so the amplitude of the recombined beam is

$$E = \frac{e^{-i\omega_c t}}{2}\{K_1 e^{i[\theta_1+\phi+m\cos(\Omega\{t-t_0\}/2)]} + K_2 e^{i[\theta_2-\phi-m\cos(\Omega\{t-t_0\}/2)]}\}. \tag{110}$$

Using the generating function of Bessel functions [12], we find that the sideband amplitudes of Eq. (24) become

$$E^{(q)} = \frac{e^{iq\Omega t_0/2}}{2}J_q(m)\{K_1 e^{i[\theta_1+\phi+q\pi/2]} + K_2 e^{i[\theta_2-\phi-q\pi/2]}\}. \tag{111}$$

Our experimental conditions are similar to those of a Mach-Zehnder modulator with perfect amplitude balance—that is, with $K_1=K_2=K$, with a mean, unbiased phase retardation $\theta=(\theta_1+\theta_2)/2$, and with a bias phase chosen for zero transmission with no microwave drive power, $(\theta_1-\theta_2)/2 + \phi = -\pi/2$. Then Eq. (111) becomes

$$E^{(q)} = e^{i(q\Omega t_0/2+\theta)}KJ_q(m)\sin(q\pi/2). \tag{112}$$

The carrier and every even sideband ($q=0,\pm2,\pm3,\dots$) are missing from the spectrum.

To provide data that could be most readily interpreted with the analysis of earlier sections of this paper, we used the push-pull pumping method [9]. For sufficiently intense light and for modulation formats close to those of the optimal waves discussed in Sec. V, push-pull pumping can concentrate most of the atoms in the superposition state of Eq. (47). For push-pull pumping, the circular polarization of the on-resonance light must alternate at a frequency Ω_m very close to the hyperfine frequency Ω of the alkali-metal atom. As in Ref. [9], we used a Michelson interferometer to split the light into two beams and to delay the phase of one with respect to the other. After emerging from the linear polarizer of Fig. 10, the FM or AM light was split into two beams, initially with the same polarization. One of the two beams was simply reflected by a mirror back to the beam splitter, while the other underwent a $\pi/2$ change in polarization, so the recombined beams from the two arms had orthogonal linear polarization. A round-trip path length difference of $\Lambda/2 = \pi c/\Omega = 2.2$ cm ensured that the recombined light beams were delayed by half a modulation period with respect to each other. The light then passed through a quarter-wave plate with its fast and slow axes oriented at 45° to the linear polarizations of the recombined beams. As discussed in Secs. II and III, the resonant light arrived at times when the absorption cross section of the atoms in the superposition state of Eq. (47) was nearly zero.

An Agilent microwave source supplied a 3.4-GHz signal to the modulators. The Mach-Zehnder modulator also required a dc bias voltage, which controlled the phase ϕ of Eq. (111). The bias was adjusted to maximize the power in the first two sidebands. Fabry-Perot spectra of the FM and AM
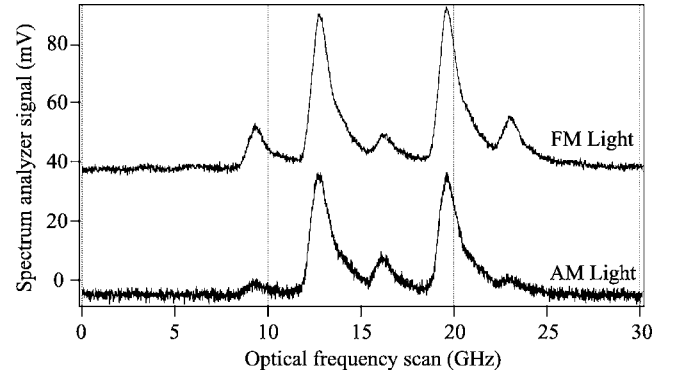

FIG. 11. Optical spectra of AM and FM pumping light, taken with the Fabry-Perot spectrum analyzer depicted in Fig. 10. The modulation indices m for the FM and AM light were about $m =1.7$ and $m=1.3$, respectively.

modulation schemes are shown in Fig. 11. The modulator parameters were adjusted to maximize the power in the two first order sidebands and to minimize the power in the carrier wave, which is undesirable because it does not participate with the first-order sidebands in generating coherence. Unfortunately, because of the amplitude imbalance ($K_1 \neq K_2$) for the Mach-Zehnder modulator, it was not possible to eliminate the carrier with the dc bias voltage.

In Fig. 12 we show raw data, the photodetector signal of Fig. 10. The bottom trace B was taken with the laser frequency tuned to the maximum of the optical absorption line. The horizontal scale is a measure of the relative tuning of the amplitude modulation frequency of the laser from the CPT resonance frequency. More light reaches the photodetector at resonance, corresponding to a partial dark state, with a substantial fraction, but not all of the atoms, in the superposition state of Eq. (47). The top trace T of Fig. 12 is the same experiment with the frequency of the laser slightly detuned from the optical resonance line. The laser power incident on the cell is nearly the same for both traces. With reference to Fig. 1, we see that the difference $T-B$ is very nearly propor-
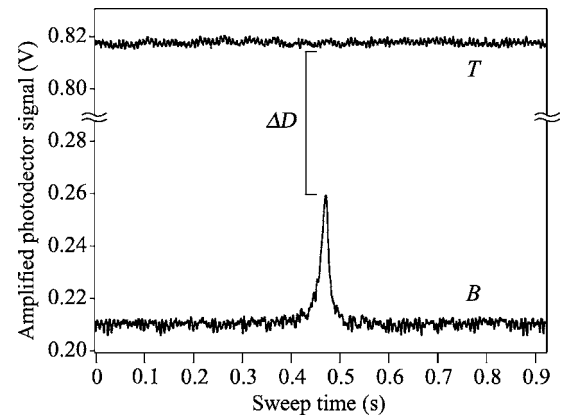

FIG. 12. CPT resonance data trace. In the lower trace, the frequency of the microwave generator is swept linearly through the resonance, covering a range of 40 kHz per second. The upper trace T is a measure of the light transmitted when the laser is detuned from the $D1$ optical resonance.
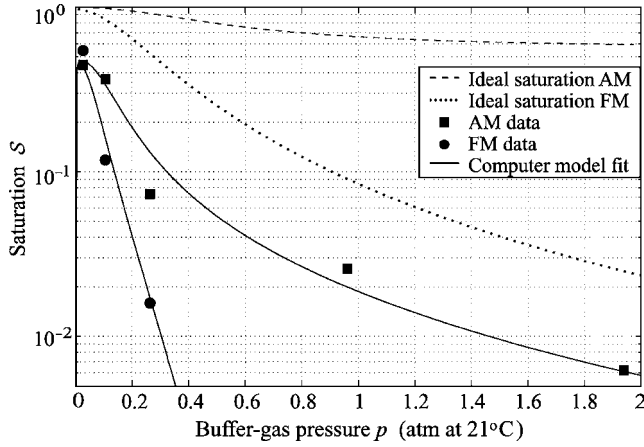
FIG. 13. CPT saturation versus buffer-gas pressure. As discussed in the text, the top two curves (dashed and dotted lines) assume that all atoms are in the superposition state of Eq. (47). The decrease in the saturation with increasing pressure comes from the optical line broadening. The CPT saturation of the experimental data (squares for AM, circles for FM) is smaller and decreases more rapidly with increasing buffer-gas pressure than for the top two, ideal curves. The two curves through the data points are from a detailed computer model that accounts for the decrease in the fraction of atoms in the superposition state and for the decrease in the optical pumping rates with increasing pressure.

tional to P_u and ΔD is proportional to P_d. The saturation of Eq. (1) is therefore

$$\mathcal{S}_{\exp} = 1 - \frac{P_d}{P_u} = 1 - \frac{\Delta D}{T - B}. \tag{113}$$

The data of Fig. 12 were uploaded to a computer, the CPT resonances were fit to Lorentzian lineshapes, and values of T, B, and ΔD were evaluated. Data were taken with cells containing room-temperature buffer-gas pressures of 20, 80, 200, 730, and 1470 Torr of N_2. The experimental saturations $\mathcal{S}_{\expt}$ from Eq. (113) are plotted in Fig. 13 as squares for AM light and circles for FM light. With AM light, CPT signals could be detected in a cell with nearly two atmospheres of N_2 buffer gas. By contrast, signals with FM light could only be detected in cells containing less than 0.3 atm.

The two curves plotted as dashed and dotted lines in Fig. 13 are ideal saturations discussed in Sec. II and given by Eq. (34) as

$$\mathcal{S} = \frac{P_1}{P_u}. \tag{114}$$

The horizontal axis is proportional to the optical line broadening γ_o of Rb atoms by buffer gas. Measurements by Romalis *et al.* [18] show that $\gamma_o/p = 5 \times 10^{10}$ s^{-1} atm^{-1} for N_2 gas of pressure p at temperatures on the order of 100 °C. The FM saturation falls off much more quickly with increasing pressure than AM. Both saturations reach their maximum value of 1 at zero pressure, since a pure superposition state was assumed in their derivation.

As can be seen from the discussion of Sec. II the mean power for FM light is

$$P_u = \mathcal{A} \sum_q \frac{J_{q+1}^2 + J_{q-1}^2}{(q\Omega/2)^2 + \gamma_o^2}, \tag{115}$$

and the phase-dependent power is

$$P_1 = -2\mathcal{A} \sum_q \frac{J_{q+1}J_{q-1}}{(q\Omega/2)^2 + \gamma_o^2}. \tag{116}$$

The Bessel functions $J_{q\pm1} = J_{q\pm1}(m)$ are summed over all integers $q = 0, \pm1, \pm2, \dots$ for the FM modulation index $m = 1.7$. $\mathcal{A}$ is the coefficient from Eq. (33).

To find the CPT saturation expected from an AM wave produced by an ideal Mach-Zehnder modulator, we use the sideband amplitudes of Eq. (112) in Eq. (28) to find the mean power

$$P_u = \mathcal{A} \sum_q \frac{J_{2q+1}^2 + J_{2q-1}^2}{(q\Omega)^2 + \gamma_o^2} \tag{117}$$

and the phase-dependent power

$$P_1 = -2\mathcal{A} \sum_q \frac{J_{2q+1}J_{2q-1}}{(q\Omega)^2 + \gamma_o^2}. \tag{118}$$

Only Bessel functions $J_{2q\pm1} = J_{2q\pm1}(m)$ with odd indices $2q \pm 1$ occur in the sum over all integers $q = 0, \pm1, \pm2, \dots$. The modulation index is $m = 1.3$.

The experimentally measured saturations $\mathcal{S}_{\expt}$ are substantially smaller than the ideal saturations. As shown in [9], the main reason is that the existing experimental setup for push-pull pumping does not concentrate all atoms into the 0-0 superposition state of Eq. (47), due to imperfect circular polarization, various spin relaxation mechanisms of the ground-state atoms, low optical pumping power, and the absence of pulse modulation. The most important relaxation mechanisms [19] which need to be considered along with the optical pumping are spin-exchange collisions between pairs of alkali-metal atoms, S damping, Carver damping [20] due to collisions between alkali-metal atoms and buffer gas atoms or molecules, and polarization losses due to diffusion to the cell walls. Increasing the buffer-gas pressure speeds up all of these relaxation mechanisms (except the last one) and also decreases the optical pumping rate because of the pressure broadening of the optical absorption line. Theoretical fits from models that take all of these effects into account are shown in the bottom two traces of Fig. 13. The fits agree well with the data.

VII. CONCLUSIONS

We have shown theoretically that the pressure dependence of 0-0 CPT resonances in alkali-metal atoms, pumped by $D1$ light, is equivalent to the absorption of a wave by a classical dipole antenna that rotates at half the 0-0 frequency. As the damping rate γ_o of the optical oscillations of the dipole or the atom increases with increasing buffer-gas pressure, CPT resonances with FM light of fixed modulation index m suffer

significant degradation. CPT resonances with AM light degrade much less quickly with increasing pressure. Optimal AM waves exist that minimize the required optical power and maximize the resonance saturation for every gas pressure. In miniature cells, high buffer-gas pressure has many advantages, including the suppression of diffusion rates and less stringent requirements on the frequency stability of the pumping light. The use of AM light offers a way to increase the buffer-gas pressure while maintaining strong CPT resonances.

[1] W. E. Bell and A. L. Bloom, Phys. Rev. Lett. **6**, 280 (1961).

[2] G. Alzetta, A. Gozzini, L. Moi, and G. Orriols, Nuovo Cimento Soc. Ital. Fis., B **36**, 5 (1976).

[3] H. R. Gray, R. M. Whitley, and C. R. Stroud, Opt. Lett. **3**, 218 (1978).

[4] E. Arimondo, *Coherent Population Trapping in Laser Spectroscopy* (North-Holland, Amsterdam, 1996), Vol. 35, pp. 257–354.

[5] J. Vanier, A. Godone, and F. Levi, Phys. Rev. A **58**, 2345 (1998).

[6] D. E. Nikonov, U. W. Rathe, M. O. Scully, S. Y. Zhu, E. S. Fry, X. F. Li, G. G. Padmabandu, and M. Fleischhauer, Quantum Opt. **6**, 245 (1994).

[7] W. Happer, Rev. Mod. Phys. **44**, 169 (1972).

[8] Z. Wu, M. Kitano, W. Happer, M. Hou, and J. Daniels, Appl. Opt. **25**, 4483 (1986).

[9] Y.-Y. Jau, E. Miron, A. B. Post, N. N. Kuzma, and W. Happer, Phys. Rev. Lett. **93**, 160802 (2004).

[10] J. Vanier, M. W. Levine, D. Janssen, and M. Delaney, Phys. Rev. A **67**, 065801 (2003).

[11] T. Zanon, S. Guerandel, E. de Clercq, D. Holleville, N. Dimarcq, and A. Clairon, Phys. Rev. Lett. **94**, 193002 (2005).

[12] *Handbook of Mathematical Functions*, Natl. Bur. Stand. Appl. Math. Ser. No. 55, edited by M. Abramowitz and I. E. Stegun (U.S. GPO, Washington, D.C., 1965).

[13] E. U. Condon and G. H. Shortley, *The Theory of Atomic Spectra* (Cambridge University Press, Cambridge, England, 1959).

[14] W. Happer and B. S. Mathur, Phys. Rev. **163**, 12 (1967).

[15] W. Franzen and A. G. Emslie, Phys. Rev. **108**, 1453 (1957).

[16] M. Stahler, R. Wynands, S. Knappe, J. Kitching, L. Hollberg, A. Taichenachev, and V. Yudin, Opt. Lett. **27**, 1472 (2002).

[17] B. A. Fuchs and B. V. Shabat, *Functions of a Complex Variable* (Addison-Wesley, Reading, MA, 1964).

[18] M. V. Romalis, E. Miron, and G. D. Cates, Phys. Rev. A **56**, 4569 (1997).

[19] Y.-Y. Jau, A. B. Post, N. N. Kuzma, A. M. Braun, M. V. Romalis, and W. Happer, Phys. Rev. Lett. **92**, 110801 (2004).

[20] D. K. Walter, W. M. Griffith, and W. Happer, Phys. Rev. Lett. **88**, 093004 (2002).